

How to measure redshift-space distortions without sample variance

Patrick McDonald*

Canadian Institute for Theoretical Astrophysics, University of Toronto, Toronto, ON M5S 3H8, Canada

Uroš Seljak

Physics and Astronomy Department and Lawrence Berkeley National Laboratory,

University of California, Berkeley, California 94720, USA and

Institute for Theoretical Physics, University of Zurich, Switzerland

(Dated: October 25, 2018)

We show how to use multiple tracers of large-scale density with different biases to measure the redshift-space distortion parameter $\beta \equiv b^{-1}f \equiv b^{-1}d \ln D / d \ln a$ (where D is the growth rate and a the expansion factor), to a much better precision than one could achieve with a single tracer, to an arbitrary precision in the low noise limit. In combination with the power spectrum of the tracers this allows a much more precise measurement of the bias-free velocity divergence power spectrum, $f^2 P_m$ – in fact, in the low noise limit $f^2 P_m$ can be measured as well as would be possible if velocity divergence was observed directly, with rms improvement factor $\sim [5.2 (\beta^2 + 2\beta + 2) / \beta^2]^{1/2}$ (e.g., $\simeq 10$ times better than a single tracer for $\beta = 0.4$). This would allow a high precision determination of fD as a function of redshift with an error as low as 0.1%. We find up to two orders of magnitude improvement in Figure of Merit for the Dark Energy equation of state relative to Stage II, a factor of several better than other proposed Stage IV Dark Energy surveys. The ratio b_2/b_1 will be determined with an even greater precision than β , producing, when measured as a function of scale, an exquisitely sensitive probe of the onset of non-linear bias. We also extend in more detail previous work on the use of the same technique to measure non-Gaussianity. Currently planned redshift surveys are typically designed with signal to noise of unity on scales of interest, and are not optimized for this technique. Our results suggest that this strategy may need to be revisited as there are large gains to be achieved from surveys with higher number densities of galaxies.

PACS numbers: 98.65.Dx, 95.35.+d, 98.80.Es, 98.80.-k

I. INTRODUCTION

Growth of structure in the universe has long been recognized as one of the most powerful ways to learn about the nature of dark energy and other properties of our universe. Currently the most promising method is weak lensing tomography, which traces the dark matter directly and can measure the growth of structure by splitting the source galaxies by their (photometric) redshift. For example, the Dark Energy Task Force concludes that of all proposed next generation experiments weak lensing holds the best promise to succeed in improving our knowledge of dark energy [1]. However, weak lensing is not necessarily the ideal method: it measures the structure projected over a broad window in redshift and its ability to probe rapid changes in growth rate is limited. Moreover, one is measuring a 2-dimensional projection only as opposed to the full 3-dimensional information, drastically reducing the amount of available information. In addition, for all of the methods proposed so far the requirements on systematic error exceed what is achievable today, so it is worth pursuing multiple methods until we have a better control of systematics.

Galaxy clustering has been the favorite method of measuring large scale structure in the universe and it is likely this will continue also in the future. The main reason is that galaxies are easily observed and that by measuring their redshift one can reconstruct the 3-dimensional clustering information, in contrast to weak lensing or cosmic microwave background anisotropies which only measure a 2-dimensional projection. The relation between galaxy and dark matter clustering is however not straight-forward. In the simplest model of linear bias galaxies trace dark matter up to an overall constant called linear bias. The bias cannot be predicted from the theory and as a result galaxy clustering alone cannot measure the growth of structure with redshift. If one could determine bias with sufficiently small error then galaxy clustering would become the leading method due to its higher information content.

There are several methods proposed to determine the bias. One is to use weak lensing, specifically galaxy-galaxy lensing which measures the cross-correlation between galaxies and dark matter. This is proportional to bias b and in combination with the galaxy auto-correlation function which scales as b^2 one can eliminate the dependence on bias

*Electronic address: pmcdonal@cita.utoronto.ca

to measure $\Omega_{m0}^2 P_m(k)$, where Ω_{m0} is the matter density parameter today and $P_m(k)$ is the matter power spectrum at a given redshift [2, 3]. Alternatively, one can also measure the halo mass distribution with weak lensing which, in connection with the theoretical bias predictions, can determine the bias and thus $P_m(k)$ [4]. A second method to determine the bias and thus $P_m(k)$ is to measure the three-point function [5]. A third method, and the one we focus here, is to measure the redshift space distortion parameter $\beta \equiv b^{-1}f \equiv b^{-1}d \ln D / d \ln a$ (where b is the bias of the galaxies, D is the linear theory growth factor, and a is the expansion factor) [6, 7, 8, 9]. In combination with the galaxy power spectrum this gives $f^2 P_m$. Note that these methods give somewhat different dynamical measurements once the bias is eliminated, so to some extent they are complementary to each other. However, none of these methods is presently competitive in terms of derived cosmological constraints, as they all have rather large statistical errors from the current data, although this may change in the future as data improve and new analysis methods are developed [10, 11, 12, 13].

In this paper we focus on redshift space distortion parameter β as a way to determine the bias. Clustering of galaxies along the line of sight is enhanced relative to the transverse direction due to peculiar motions and this allows one to determine β . Current methods require one to compare the clustering strength as a function of angle relative to the line of sight, but this method is only applicable on large scales where linear theory holds. As a result, the sampling variance limits its statistical precision. Recently, [14] proposed a new method for measuring the primordial non-Gaussianity parameter f_{NL} , by comparing two sets of galaxies with a different bias, and a different sensitivity to f_{NL} [15], which allows one to eliminate the sample variance. Optimization of this technique was investigated by [16]. Here we apply this technique to the measurement of the redshift-space distortion parameter, which in turn improves the measurement of the velocity divergence power spectrum $P_{\theta\theta} \equiv f^2 P_m(k)$. As we show here, this approach can in principle measure β perfectly and $P_{\theta\theta}$ as well as if we observed velocity divergence directly. If this promise were realized from the data it would allow for a much higher statistical power than weak lensing or other 2-dimensional projections. We also show that our method, and large-scale structure surveys in general, become even more powerful when additional cosmology dependence, such as the Alcock-Paczyński effect [17], is included.

We begin by presenting the basic method, followed by an analysis of the expected improvement as a function of survey parameters. This is followed by predictions for some of the existing and future surveys in terms of expected improvement of dark energy parameters. On small scales the deterministic linear bias model eventually becomes inaccurate and for this reason we often quote results as a function of the maximum usable wavenumber, k_{max} . While we have some idea what its value should be, we leave a more detailed analysis with numerical simulations for the future. One should note, however, that the multiple-tracer approach is likely to actually help in disentangling non-linear bias effects on quasi-linear scales, making those scales potentially much more useful than they would otherwise be. We conclude with a summary and a discussion of future directions.

II. METHOD AND RESULTS

The density perturbation, δ_{gi} , for a type of galaxy i , in the linear regime, in redshift space, is [18]

$$\delta_{gi} = (b_i + f\mu^2) \delta + \epsilon_i \quad (1)$$

where b_i is the galaxy bias, $\mu = k_{\parallel}/k$, δ is the mass density perturbation, and ϵ_i is a white noise variable which can represent either the standard shot-noise or other stochasticity. All equations are understood to apply to the real or imaginary part of a single Fourier mode unless otherwise indicated. In this paper we will consider two types of galaxies, type 1 with bias b , and type 2 with bias αb . The perturbation equations can then be written

$$\delta_{g1} = f(\beta^{-1} + \mu^2) \delta + \epsilon_1, \quad (2)$$

and

$$\delta_{g2} = f(\alpha\beta^{-1} + \mu^2) \delta + \epsilon_2. \quad (3)$$

We are denoting $\beta = f/b$ (the equivalent distortion parameter for the 2nd type of galaxy is β/α).

The traditional method to determine β is to look at the angular dependence of the two-point correlation function or its Fourier transform, the power spectrum. The correlations will be enhanced along the line of sight (where $\mu = 1$) relative to the direction perpendicular to it (where $\mu = 0$), but to observe this enhancement one must average over many independent modes to beat down the sampling (or cosmic) variance. This is because each mode is a random realization of a Gaussian field and there will be fluctuations in the measured power even in the absence of noise. By combining a measurement of β with that of the galaxy power spectrum one can determine $f^2 P_m$, which no longer depends on the unknown bias of the galaxies. This method has been applied to the data, most recently in [6, 7, 8, 9],

and is limited by the accuracy with which we can determine β . For example, for the analysis in [8], which currently has the highest signal to noise measurement of β , the error on the overall amplitude of galaxy power spectrum P_{gg} is about 1% adding up all the modes up to $k = 0.1 h \text{ Mpc}^{-1}$, while the error on β is about 12%, so the error on reconstructed $f^2 P_m = \beta^2 P_{gg}$ is entirely dominated by the error on β . Predictions for the future surveys with this and related methods can be found in [12, 13].

To understand the main point of the new method we are proposing here let us consider the situation without the noise, which would apply if, for example, we have a very high density of the two tracers sampling the field, and no stochasticity. In that case we can divide equation 3 by equation 2 above to obtain

$$\frac{\delta_{g2}}{\delta_{g1}} = \frac{\alpha\beta^{-1} + \mu^2}{\beta^{-1} + \mu^2}. \quad (4)$$

This expression has a specific angular dependence, allowing one to extract α and β separately. Note that there is no dependence on the density field δ . The random nature of the density field is therefore not affecting this method and we can determine β exactly in the absence of noise. More generally, the precision with which we can determine β is controlled by the (shot) noise, i.e. density of tracers, rather than the sampling variance. In order to address the gains in a realistic case we must perform the full analysis, which we turn to next.

Generally, the noise variables can be correlated with each other, although they would not be for standard shot-noise. For example, [19] showed that one generically expects non-linear structure formation to generate a full covariance matrix for the noise at some level, so this will probably be the ultimate limit for this kind of measurement. The covariance matrix of the perturbations is

$$C \equiv \begin{bmatrix} \langle \delta_{g1}^2 \rangle & \langle \delta_{g1} \delta_{g2} \rangle \\ \langle \delta_{g2} \delta_{g1} \rangle & \langle \delta_{g2}^2 \rangle \end{bmatrix} = \frac{P_{\theta\theta}}{2} \begin{bmatrix} (\beta^{-1} + \mu^2)^2 & (\beta^{-1} + \mu^2)(\alpha\beta^{-1} + \mu^2) \\ (\beta^{-1} + \mu^2)(\alpha\beta^{-1} + \mu^2) & (\alpha\beta^{-1} + \mu^2)^2 \end{bmatrix} + \frac{N}{2} \quad (5)$$

where $P_{\theta\theta} \equiv 2f^2 \langle \delta^2 \rangle$ and $N_{ij} \equiv 2 \langle \epsilon_i \epsilon_j \rangle$ (note that $P_{\theta\theta}$ and N are the usual power spectrum and noise – the factor of 2 comes from the fact that δ and ϵ are only the real or imaginary part of a Fourier mode). If we assume that the noise matrix is known then the covariance matrix for two types of galaxies is a function of three parameters: the velocity divergence power spectrum amplitude, $P_{\theta\theta}$, the redshift-space distortion parameter, β , and the ratio of biases α . We work with α instead of a second β parameter because the ratio of biases will generally be determined substantially more precisely than β , which means that the measurement of the second β parameter would be almost perfectly correlated with the first. The Fisher matrix for the measurement of these parameters is

$$F_{\lambda\lambda'} = \frac{1}{2} \text{Tr} [C_{,\lambda} C^{-1} C_{,\lambda'} C^{-1}] \quad (6)$$

where $C_{,\lambda} \equiv dC/d\lambda$ and λ are the parameters.

For any single mode, the inverse of the Fisher matrix is singular, i.e., we can only constrain two parameters, not three. However, adding Fisher matrices for modes with different μ breaks this degeneracy. Generally, the total Fisher matrix will be an integral over modes with all angles. As a simple example, we assume first a pair of modes with $\mu = 0$ and $\mu = 1$ and compute the error on the parameters in the small noise limit:

$$\frac{\sigma_\alpha^2}{\alpha^2} = X_{11} - 2X_{12} + X_{22}, \quad (7)$$

where $X_{ij} = N_{ij}/b_i b_j P_m$,

$$\frac{\sigma_\beta^2}{\beta^2} = \frac{\left[\alpha^2 (1 + \beta)^2 + (\alpha + \beta)^2 \right] X_{11} - 2 \left[\alpha^2 (1 + \beta)^2 + \alpha (1 + \beta) (\alpha + \beta) \right] X_{12} + 2\alpha^2 (1 + \beta)^2 X_{22}}{\beta^2 (\alpha - 1)^2}, \quad (8)$$

and

$$\frac{\sigma_{P_{\theta\theta}}^2}{P_{\theta\theta}^2} = 1. \quad (9)$$

The key points are that the only lower limit on the errors on α and β from this single pair of modes is set by the achievable noise-to-signal ratios on the tracers, X_{ij} , and the error on $P_{\theta\theta}$ is the error one would obtain for a simple power spectrum measurement from two modes, with no degradation due to degeneracy with the bias parameters (this is of course only true to leading order in the small noise limit).

In contrast, for a single type of galaxy, for the same pair of radial and transverse modes, in the low noise limit we find:

$$\frac{\sigma_\beta^2}{\beta^2} = \frac{(1 + \beta)^2}{\beta^2} \quad (10)$$

and

$$\frac{\sigma_{P_{\theta\theta}}^2}{P_{\theta\theta}^2} = \frac{2(\beta^2 + 2\beta + 2)}{\beta^2} \quad (11)$$

i.e., here the signal-to-noise per mode on β saturates at greater than unity for low noise, and the overall power measurement is substantially degraded because we cannot determine β very accurately and this then limits the precision with which the velocity divergence power spectrum can be determined as well. If we assume the first tracer is much better sampled than the second, we get the ratio of errors

$$\frac{\sigma_\beta^2 (2 \text{ tracers})}{\sigma_\beta^2 (1 \text{ tracer})} \simeq \frac{2\alpha^2 X_{22}}{(\alpha - 1)^2} = \frac{2N_{22}}{(b_2 - b_1)^2 P_m} \quad (12)$$

and

$$\frac{\sigma_{P_{\theta\theta}}^2 (2 \text{ tracers})}{\sigma_{P_{\theta\theta}}^2 (1 \text{ tracer})} \simeq \frac{\beta^2}{2(\beta^2 + 2\beta + 2)} \quad (13)$$

We see that the improvement in the measurement of β can be arbitrarily large in the limit $N_{22} \rightarrow 0$, while the improvement in $P_{\theta\theta}$ is limited by sample variance but is generally quite large, e.g., a factor $10^{1/2}$ (rms) for $\beta = 1$, and $50^{1/2}$ for $\beta = 1/3$. All of these formulae are only good as long as the noise is small relative to the power spectrum of the difference between the two tracer fields (obviously the two tracer case should never be worse than the one tracer case).

A yet more realistic analysis must integrate over all modes rather than look just at the two specific modes as done above. In doing so we find that the two-mode approximation above substantially underestimates the improvement in the $P_{\theta\theta}$ measurement. If we integrate the Fisher matrix over the full range of μ , the improvement is a factor of approximately $2.6^{1/2}$ larger than above, e.g., a factor of $25^{1/2}$ for $\beta = 1$, or $138^{1/2}$ for $\beta = 1/3$. The result of the μ integration in the idealized case of two perfect tracers remains simply:

$$\frac{\sigma_{P_{\theta\theta}}^2}{P_{\theta\theta}^2} = \frac{2}{N}, \quad (14)$$

where N is the effective number of discrete modes sampled (counting real and imaginary parts separately). Thus, the combination of two perfect tracers produces the measurement of $f^2 P_m$ that one would obtain if one could observe the velocity divergence field directly and perfectly.

A. General usefulness of redshift-space distortion measurements

Of course, we will never have perfect sampling, so it is necessary to numerically evaluate the exact Fisher matrix with finite noise to determine the improvement for real surveys. We assume the survey volume, V , is roughly spherical, so the Fisher matrix for a survey will be

$$F_V \simeq \frac{V}{4\pi^2} \int_{k_{\min}}^{k_{\max}} k^2 dk \int_{-1}^1 d\mu F(k, \mu) \quad (15)$$

where $F(k, \mu)$ is computed for a single mode using Eqs. (5) and (6) (remembering that both real and imaginary parts must be added). We assume the minimum usable k is $k_{\min} \simeq 2\pi/V^{1/3}$.

In Figure 1 we show the errors on the amplitude of the velocity divergence power spectrum $P_{\theta\theta}$ that one can obtain from a generic 3/4-sky (30000 square degree) survey, as a function of redshift. This may seem unreasonably optimistic/futuristic, but it may be possible surprisingly quickly if the 21 cm emission intensity mapping method is successful [20], as discussed further below. We assume either $k_{\max}(z) = 0.1 [D(z)/D(0)]^{-1} h \text{ Mpc}^{-1}$, or $k_{\max}(z) = 0.05 [D(z)/D(0)]^{-1} h \text{ Mpc}^{-1}$, with the redshift dependence motivated by [21, 22]. We give results for different values

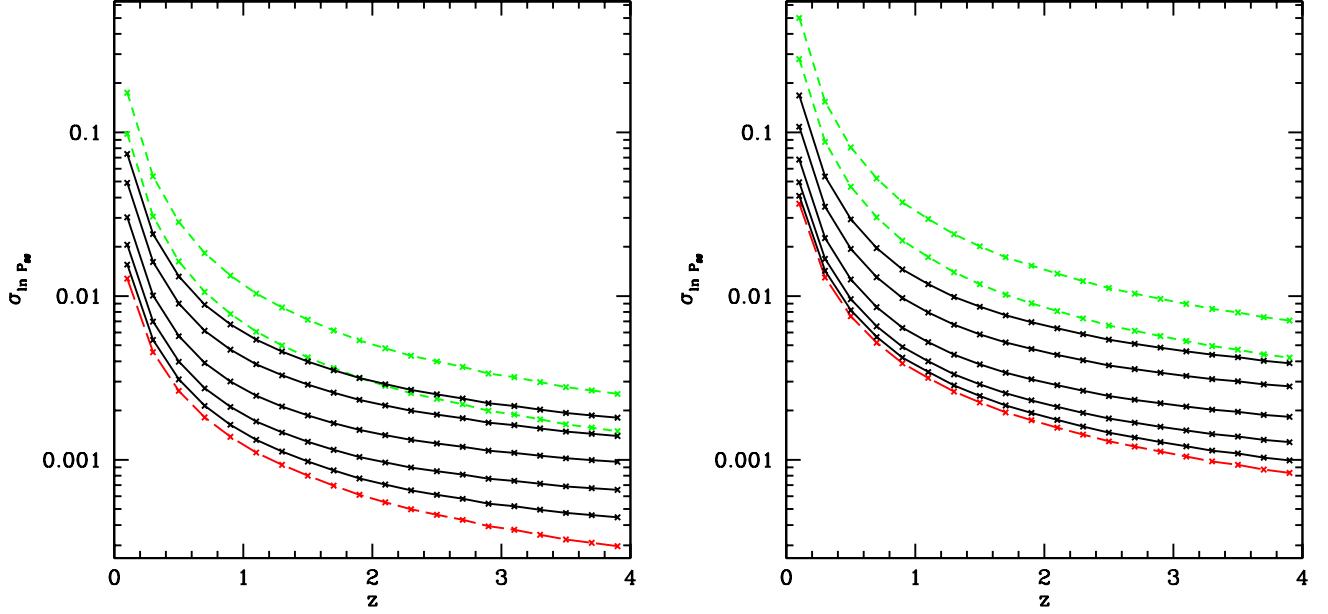


FIG. 1: Projected fractional error on the normalization of $P_{\theta\theta} \equiv f^2 P_m$, for 30000 square degrees, in redshift bins with width $dz = 0.2$. The upper and lower green (short-dashed) lines show the constraints from single tracers with $b = 2$ and $b = 1$, respectively. Black (solid) lines show the two tracers together, each with, from top to bottom, $S/N=1, 3, 10, 30, 100$ at $k = 0.4 h \text{ Mpc}^{-1}$. The red (long-dashed) line shows the case where both tracers are perfectly sampled. For the left panel we assume $k_{\text{max}}(z) = 0.1 [D(z)/D(0)]^{-1} h \text{ Mpc}^{-1}$, while the right assumes $k_{\text{max}}(z) = 0.05 [D(z)/D(0)]^{-1} h \text{ Mpc}^{-1}$.

of X_{ij} at $k = 0.4 h \text{ Mpc}^{-1}$ (for $i = j$, i.e., the off-diagonal element is zero). Surveys with $S/N \sim 1$ at $k = 0.4 h \text{ Mpc}^{-1}$ recover $\sim 90\%$ of the total possible information from BAO measurements, i.e., the S/N ratios we give should be interpreted as being relative to a nearly ideal BAO survey. In these calculations we are assuming the shape of the power spectrum is known so that we can compress the information from all the modes into a single number, that of the power spectrum amplitude. This is discussed further below.

We see from Fig. 1 that one obtains large improvements using the multi-tracer method, even for S/N as small as 3. For example, at $z \sim 1$, with $k_{\text{max}}(z) = 0.1 [D(z)/D(0)]^{-1} h \text{ Mpc}^{-1}$, the gain is equivalent to increasing the survey volume by a factor of 3 over a single, perfectly sampled, unbiased tracer. For the more conservative $k_{\text{max}}(z)$, the results are substantially degraded, but the multi-tracer method actually becomes more valuable, at fixed absolute S/N level, because the S/N level in the usable range of k is higher.

It is interesting to note that, in the single-tracer case, low bias is substantially better than high bias. This is easy to understand from Eq. 1 – lower bias simply means that power due to redshift-space distortions makes a larger fractional contribution to the total. The practical consequence of this observation is that, once BAO surveys using high bias objects have been completed, an opportunity exists for improvement by observing lower bias objects at similarly low S/N , i.e., even if the S/N is not large enough to decisively exploit the multi-tracer method in this paper.

To put these results into a broader context, Fig. 2 shows how velocity divergence power spectrum $P_{\theta\theta} = f^2 P_m$ depends on the underlying cosmological parameters of interest, as a function of redshift. The derivatives with respect to parameter p_i , $d \ln P_{\theta\theta} / dp_i$, are taken at fixed values of the other parameters in the following set: $\omega_m = \Omega_m h^2$, the matter density; $\omega_b = \Omega_b h^2$, the baryon density; θ_s , the angle subtended by the sound horizon at the CMB decoupling redshift; w_0 and w' , defined by $w(z) = w_0 + w'(1 - a) = p(z)/\rho(z)$ where here $p(z)$ and $\rho(z)$ are the dark energy pressure and density; Ω_k , the effective fraction of the critical density in curvature; and A and n_s , the amplitude and power law slope of the primordial perturbation power spectrum. Fixing ω_m , ω_b , θ_s , A , and n_s guarantees that changes in w_0 , w' , and Ω_k have minimal effect on the CMB. The scale for the parameter dependences is chosen using the error bars on each parameter that we project for the scenario described for Fig. 5, including the Planck CMB experiment, and $P_{\theta\theta}$ and BAO constraints up to $z_{\text{max}} = 1$. While it is easy to see that $P_{\theta\theta}$ measurements have a lot of power to constrain parameters, especially the dark energy equation of state, exactly what constraints can be obtained is not obvious to the eye, because one needs to account for degeneracy between parameters.

In the derivatives in Fig. 2, and the following calculations, we assume that the constraints on $P_{\theta\theta}$ can be taken as a

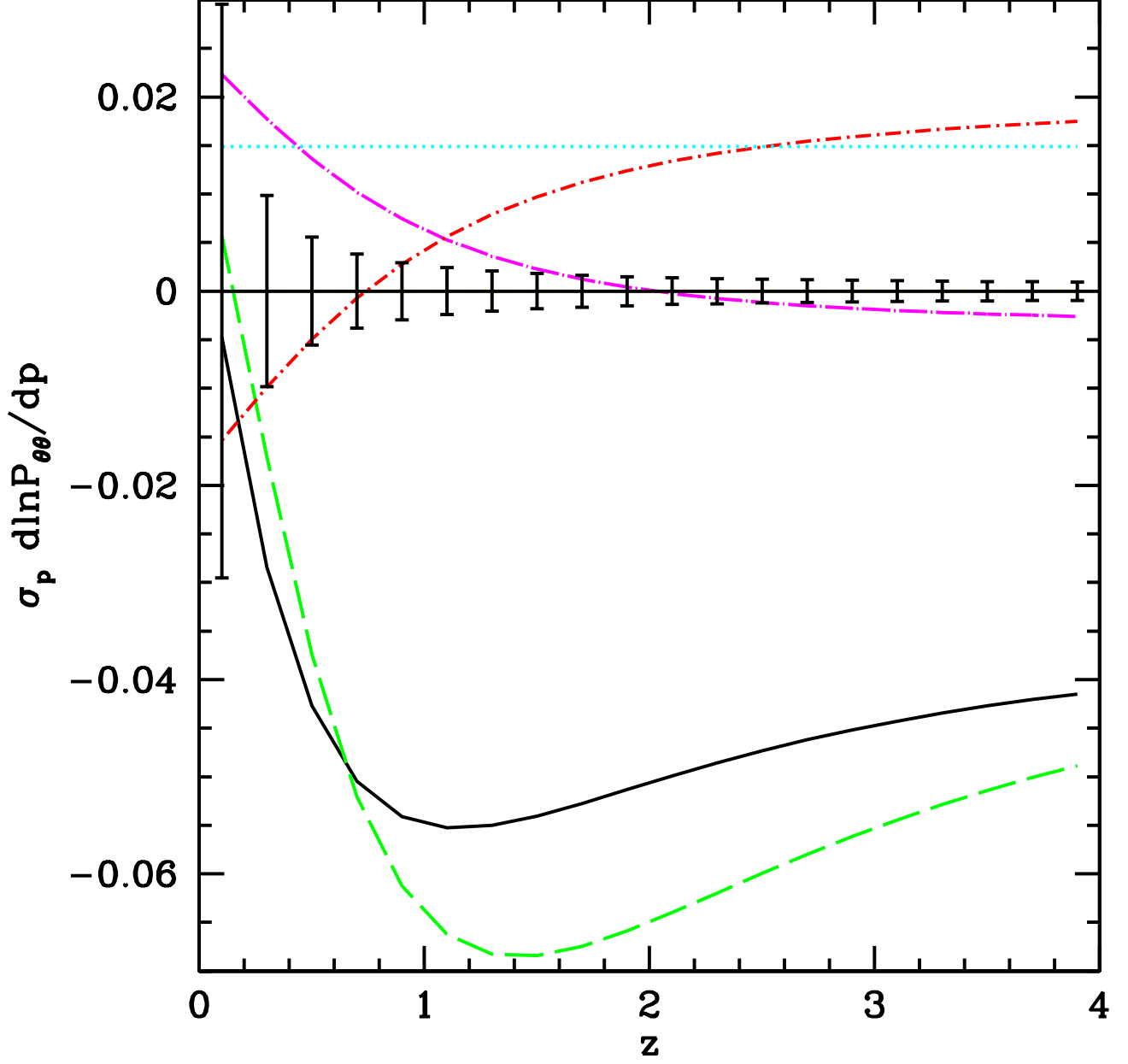


FIG. 2: Dependence of $P_{\theta\theta}$ ($k = 0.1 \, h \, \text{Mpc}^{-1}$, z) on cosmological parameters. The derivatives are at fixed values of the other parameters, including not-shown parameters ω_b , θ_s , and n_s . The derivatives are normalized by typical projected errors on the parameters, for the scenario described in Fig. 5, with $z_{\text{max}} = 1$. Lines correspond to: black (solid): w_0 , green (long-dashed): w' , red (dot-short-dashed): Ω_k , magenta (dot-long-dashed): ω_m , cyan (dotted): $\log A$. Error bars show the projected errors on $P_{\theta\theta}$ for $k_{\text{max}}(z) = 0.1 \, [D(z)/D(0)]^{-1} \, h \, \text{Mpc}^{-1}$, and $S/N = 10$.

measurement of $P_{\theta\theta}$ at $k = 0.1 \, h \, \text{Mpc}^{-1}$, for all z and all cosmological models. This allows us to apply the constraints directly to the product $f(z)D(z)$, with the power spectrum entering only through a single overall normalization. We do this for simplicity and transparency (i.e., so one can see clearly where the constraints are coming from), but it is imperfect in two ways: first, the measurement at different redshifts is really weighted toward different k , so the shape of the power spectrum enters in converting between them; and, second, we can not measure the power spectrum in $h^{-1} \, \text{Mpc}$ units, only radial velocity separations and angular separations, which leads to sensitivity to the Hubble

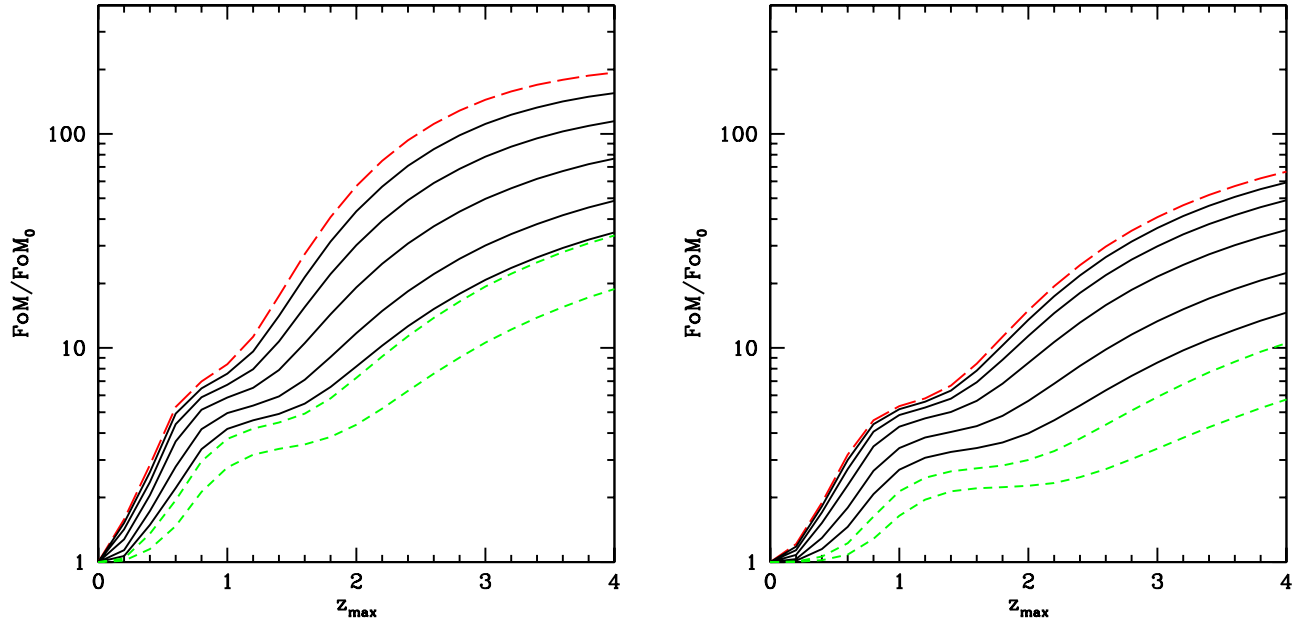


FIG. 3: Improvement in Dark Energy constraints (quantified by the DETF FoM), relative to Planck + DETF Stage II, when the $P_{\theta\theta}$ constraints from Fig. 1 are added. The lines refer to the same cases as in Fig. 1, and again the left panel is $k_{\max}(z) = 0.1 [D(z)/D(0)]^{-1} h \text{ Mpc}^{-1}$ while the right is $k_{\max}(z) = 0.05 [D(z)/D(0)]^{-1} h \text{ Mpc}^{-1}$.

parameter, $H(z)$, and angular diameter distance, $D_A(z)$ (this includes, but is not entirely, the Alcock-Paczyński effect [17]). We will revisit these issues later.

In Fig. 3 we show the contribution these measurements of $P_{\theta\theta}$ can make to the study of dark energy, quantified by the Dark Energy Task Force (DETF) Figure of Merit (FoM), proportional to the inverse of the area within the 95% confidence contours describing constraints on w_0 and w' [1]. We see that there is the potential for a huge improvement in dark energy constraints, by two orders of magnitude in the FoM, when $k_{\max}(z) = 0.1 [D(z)/D(0)]^{-1} h \text{ Mpc}^{-1}$, well beyond even the optimistic Stage IV constraints envisioned by the DETF (which gave an improvement of a factor ~ 20 in the units of this figure). The FoM improvements for the $k_{\max}(z) = 0.05 [D(z)/D(0)]^{-1} h \text{ Mpc}^{-1}$ constraints are substantially weaker of course, but still potentially spectacular.

Finally, we add the BAO distance measurements that one would obtain from the same surveys, with the resulting FoM shown in Fig. 4. We see that even a minimal $P_{\theta\theta}$ measurement adds substantially to the BAO-only measurement. To give more meaning to these FoM improvement numbers: in the best case shown here, the constraint on $w(z_p)$ at the pivot point $z_p \simeq 0.8$ (where the errors on $w(z_p)$ and w' are uncorrelated) is ± 0.0023 , with w' is measured to ± 0.031 . In the less optimistic case of $S/N = 10$ out to $z_{\max} = 2$, with $k_{\max}(z) = 0.1 [D(z)/D(0)]^{-1} h \text{ Mpc}^{-1}$, we find $w(z_p = 0.45)$ is constrained to ± 0.0074 , and w' to ± 0.091 .

Finally, in Fig. 5 we show the constraints on all of the parameters where $P_{\theta\theta}$ helps significantly, not just dark energy. This figure is for the specific case with Planck, Stage II, BAO from the same galaxy survey included, $k_{\max}(z) = 0.1 [D(z)/D(0)]^{-1} h \text{ Mpc}^{-1}$, and $S/N=10$ (note that, with one exception that we will indicate, k_{\max} generally does not apply to the BAO calculation, which essentially follows the procedure in [22]). We see that dramatic improvements will be made in the constraints on Ω_k , Ω_Λ (the dark energy density), and even ω_m and A .

B. Specific example surveys

We now explore a few planned or existing surveys.

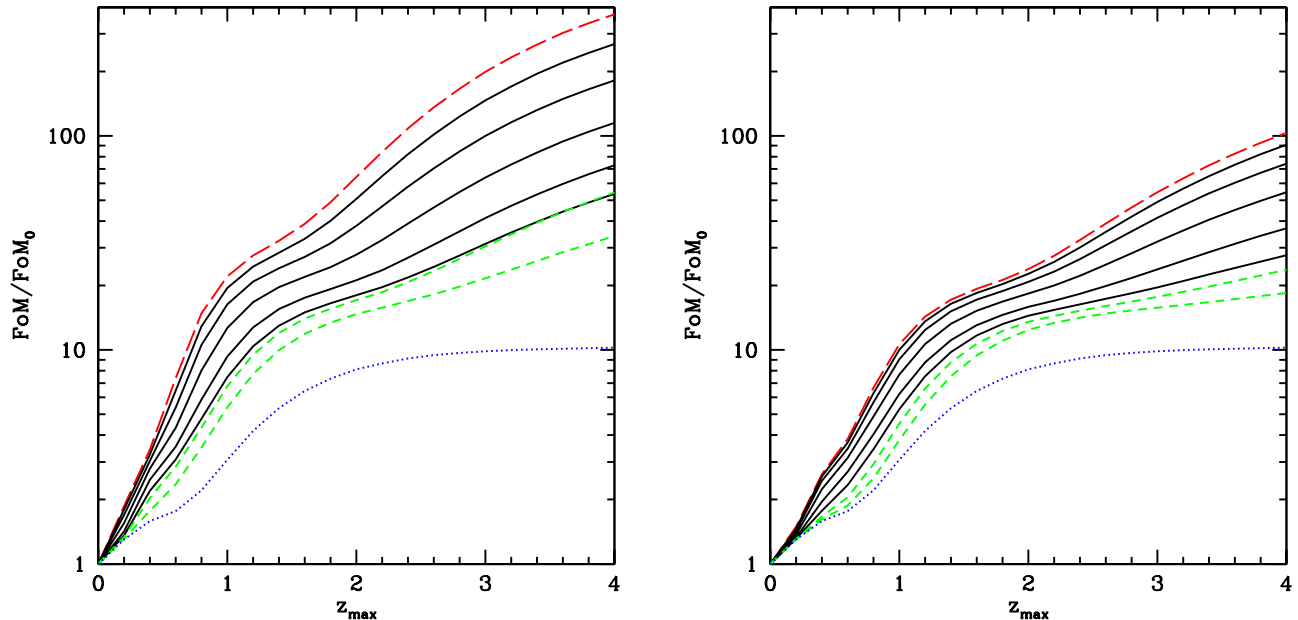


FIG. 4: Improvement in Dark Energy constraints (quantified by the DETF FoM), relative to Planck + DETF Stage II, when the $P_{\theta\theta}$ constraints from Fig. 1 are added, and the BAO distance measurements from the same survey is added. The lines refer to the same cases as in Fig. 1, except the blue (dotted) line is the case with BAO alone. The left and right panels again show the stronger and weaker values of k_{\max} , respectively.

1. High redshift, high volume space mission

As a first example, we consider scenarios motivated by the EUCLID mission [23] (EUCLID is the combination of the missions formerly known as SPACE and DUNE – there is a proposal similar to SPACE in the USA named ADEPT). The proposal is to cover $\sim 1/2$ of the sky over a wide range of redshifts. Our calculation considers $100 (h^{-1}\text{Gpc})^3$ centered at $z = 1.4$. We use the planned galaxy density $0.0016 (h^{-1}\text{Mpc})^{-3}$ (L. Guzzo, private communication). We assume a mean bias of $b = 2$ (somewhat arbitrarily – the bias could be significantly higher if one is able to select galaxies in the most massive halos at that time). Fig. 6 shows the $f^2 P_m$ measurement for various modifications or additions to the EUCLID mission. We see (black, solid line, in the upper left) that this survey is a long way from achieving the best possible measurement of $P_{\theta\theta}$, by almost a factor of 10 in the rms error. Viewed as a single tracer, the problem is not noise (compare to the magenta, dotted line), it is simply that, for $b = 2$, we lose this much constraining power to degeneracy with the bias. A single perfectly sampled tracer with $b = 1$ would do better, but still be far from as good as possible (blue, dot-dashed). If we hypothetically split the sample into $b = 1.5$, $\bar{n} = 0.0008 (h^{-1}\text{Mpc})^{-3}$ and $b = 2.5$, $\bar{n} = 0.0008 (h^{-1}\text{Mpc})^{-3}$ subsamples (chosen for illustration, not because we know this is possible), in order to exploit the method of [14], the gains are non-negligible, especially on large scales where they can more than double the effective volume of the survey, however, the noise is too large to achieve the much larger gains that are in principle possible. If we could leave the EUCLID-like sample intact and add a perfect unbiased tracer as the second field, we would get a substantial gain from the combination, equivalent to multiplying the volume of the survey by a factor of $\sim 10 - 17$ (the exact improvement factor depends on k_{\max}), although a factor ~ 3 of this would be obtained from the perfect unbiased tracer alone. As a practical matter, a factor of ten larger number density for the unbiased tracer over the biased tracer is nearly equivalent to perfect, i.e., the rms error is within $\sim 10\%$ of the infinite density error.

The ratios shown in the upper left of Fig. 6 are largely independent of the volume of the survey. The upper right of Fig. 6 shows how well one can do in an absolute sense with a 100 cubic Gpc/h survey. One critical point to take away from this figure is how vital it is to push k_{\max} to be as large as possible. The overall error on a power spectrum scales like k_{\max}^3 as long as one has good S/N, so a mere 30% slippage in k_{\max} (e.g., $0.1 h \text{ Mpc}^{-1}$ instead of $0.13 h \text{ Mpc}^{-1}$) is equivalent to throwing away more than half of the survey volume! Similarly, when one is using the multi-tracer method in this paper, increasing k_{\max} by a factor of two is roughly equivalent to an order of magnitude increase in

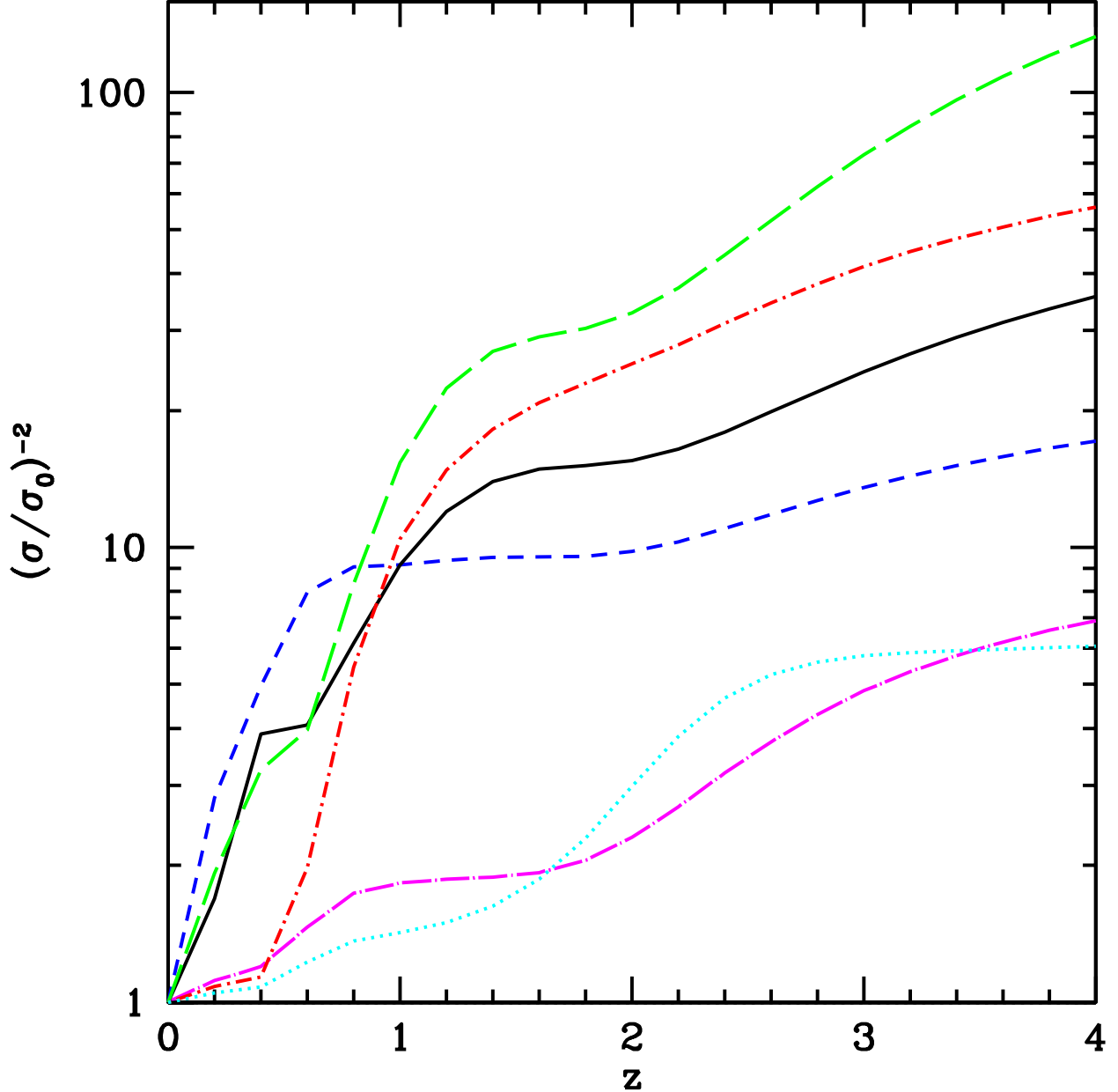


FIG. 5: Improvements in constraints on various parameters, vs. z_{\max} , for the case including BAO, $k_{\max}(z) = 0.1 [D(z)/D(0)]^{-1} h \text{ Mpc}^{-1}$, and $S/N = 10$ for the $P_{\theta\theta}$ measurement. Lines are: black (solid): w_0 , green (long-dashed): w' , red (dot-short-dashed): Ω_k , blue (dashed): Ω_Λ , magenta (dot-long-dashed): ω_m , cyan (dotted): $\log A$.

the number of galaxies. Future analyses will need to explore k_{\max} of the single versus double tracer method, but for this numerical simulations are needed, which are beyond the scope of this paper.

Figure 6 also shows the projected error on β , which shows very similar dependences to $f^2 P_m$. In fact, the β and $f^2 P_m$ errors are almost perfectly correlated, to the point where it is probably most accurate to think of these surveys as making a very precise measurement of $b^2 P_m$ which is converted to $f^2 P_m$ by multiplying by β^2 , with the resulting error dominated by the error on β . Note, however, that with very low noise, the β error will continue to decrease toward zero, while the $b^2 P_m$ error will not and therefore will eventually dominate the $f^2 P_m$ error (of course, this is just the cosmic variance limit for a direct measurement of velocity divergence). Fig. 6 also shows the projected error

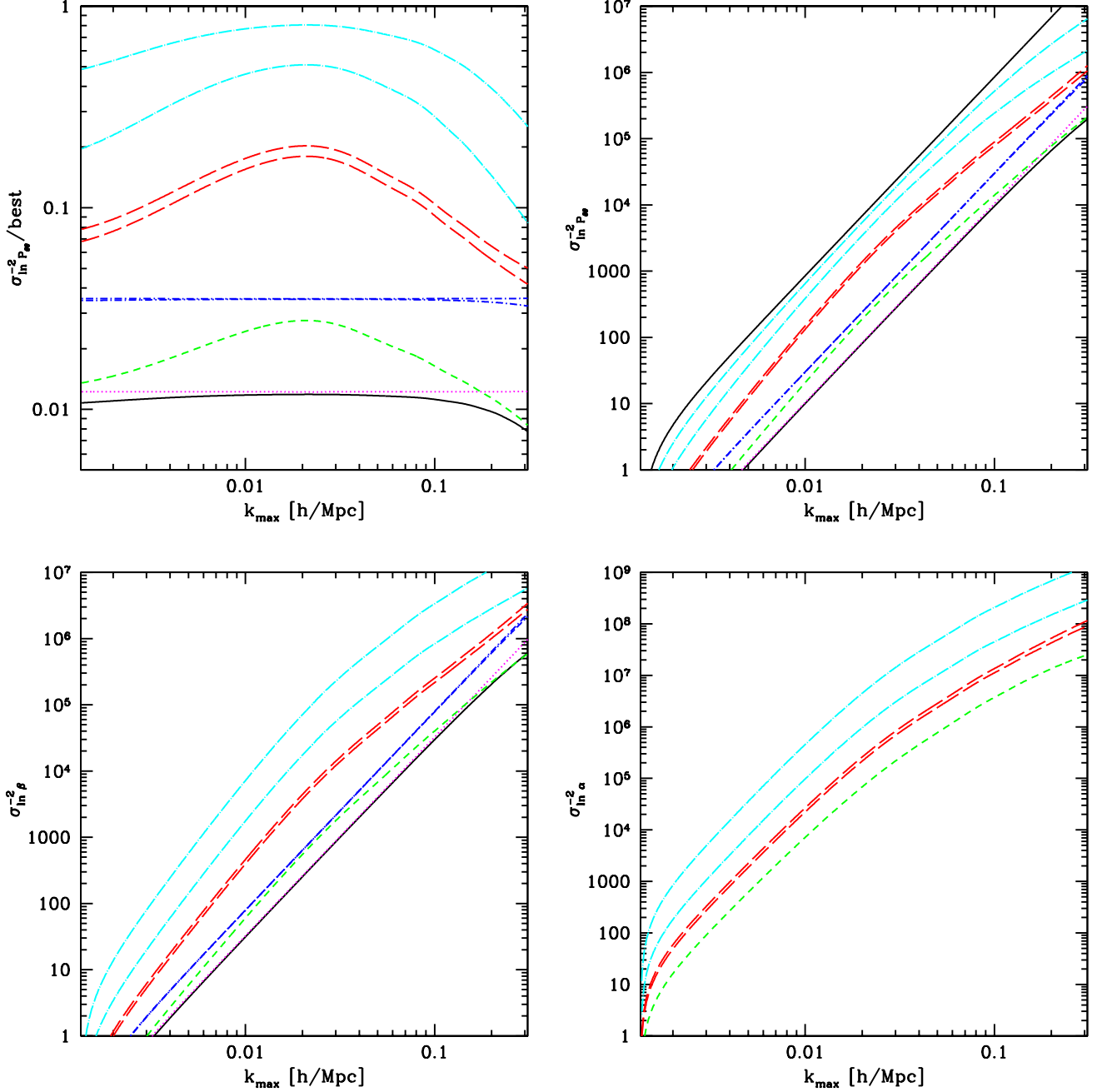


FIG. 6: Upper left panel: Projected error (inverse variance) on the normalization of $P_{\theta\theta} \equiv f^2 P_m$, relative to the error one could achieve by observing velocity divergence directly (which is also obtainable by observing two noise-free tracers with different bias), as a function of k_{\max} , for the EUCLID mission-motivated example described in the text. The black (solid) line shows EUCLID-like galaxies treated as a single tracer. The magenta (dotted) and blue (dot-short-dashed) lines show single perfectly sampled tracers with $b = 2$ and $b = 1$, respectively. Green (short-dashed) shows the EUCLID-like galaxies split into two groups with different bias, as described in the text. Red (long-dashed) shows the EUCLID-like galaxies plus a perfect unbiased tracer, while cyan (dot-long-dashed) shows a density $\bar{n} = 0.03 \text{ (h}^{-1} \text{ Mpc)}^{-3}$ plus an unbiased tracer. Where there are two lines of the same type, the upper one uses a genuinely perfectly sampled tracer, while the lower one shows density $\bar{n} = 0.03 \text{ (h}^{-1} \text{ Mpc)}^{-3}$. Because the error is always dominated by k 's near k_{\max} , this plot (and subsequent plots) also gives a good estimate of how well one can do near k_{\max} in a scale dependent measurement. Upper right panel: Projected absolute error on $P_{\theta\theta}$ for the same cases, except the upper black (solid) curve is for perfectly observed velocity divergence (or two perfect tracers with different bias). Lower left (right) panel: Projected error on β (α), which has no cosmic variance limit.

on α . α can be measured very precisely, e.g., even for the simple split of the EUCLID-like sample in half, α will be measured to $\sim 0.1\%$ for $k_{\max} = 0.05 h \text{ Mpc}^{-1}$, and $\sim 1\%$ for $k_{\max} \gtrsim 0.01 h \text{ Mpc}^{-1}$. This will measure the scale dependence of α and thus allow a very precise test of the onset of non-linear biasing.

2. Higher density, smaller volume space mission

Another option to consider is a space mission with a somewhat smaller volume, but higher density of galaxies. For example, one of the SNAP satellite designs would allow for a 10000 sq. deg. survey at $0.9 < z < 1.6$, with density $\bar{n} = 0.004 (h^{-1} \text{ Mpc})^{-3}$ and mean bias $b = 2.3$ (D. Schlegel, private communication). The higher density than EUCLID is what we look for to make the multiple-tracer method powerful. We show projections in Fig. 7. As an example, we split the SNAP sample into $b = 2.8$ and $b = 1.8$ subsamples. The improvement in $P_{\theta\theta}$ measurement is substantial, a factor of $\sim 2 - 5$ in effective volume, depending on k_{\max} . The enhanced density of SNAP over EUCLID would roughly cancel the factor of 2 in greater sky area in the EUCLID survey (note, however, that the EUCLID survey still comes out ahead overall because it covers a broader redshift extent).

3. SDSS-III/BOSS

Fig. 8 shows the achievable gains for survey configurations motivated by the SDSS-III/BOSS survey [32]. BOSS will cover 10000 sq. deg. with central redshift $z = 0.5$ and maximum $z \sim 0.7$, giving comoving volume 6 cubic Gpc/h. The planned galaxy sample has $b \sim 1.9$ and number density $\bar{n} = 0.0003 (h^{-1} \text{ Mpc})^{-3}$. Not coincidentally, the form of Fig. 8 is very similar to Fig. 6. The only quantity that really matters for these calculations is the basic ratio of the noise level to power spectrum level, and the optimization of these surveys for BAO means that this ratio will be very similar. The BOSS S/N is somewhat lower than EUCLID, so BOSS is even farther from achieving the best possible measurement of $P_{\theta\theta}$. If we hypothetically split the sample into a $b = 1.6$, $\bar{n} = 0.0002 (h^{-1} \text{ Mpc})^{-3}$ and $b = 2.5$, $\bar{n} = 0.0001 (h^{-1} \text{ Mpc})^{-3}$ subsamples (chosen for illustration, not because this is known to be possible), in order to exploit the method of [14], the gains are small – the noise is too large. The different panels of Fig. 8 show how well one can do in an absolute sense with a 6 cubic Gpc/h survey, on $P_{\theta\theta}$, β , and α .

4. Present SDSS

To put the future in context, it is interesting to see what we could do with current SDSS data. First, we take the LRGs, which we assume cover 2 cubic Gpc/h centered at $z \sim 0.33$ (10000 sq. deg.) with a density $\bar{n} = 0.000068 (h^{-1} \text{ Mpc})^{-3}$, and $b = 1.9$. Fig. 9 shows our usual comparison between the $P_{\theta\theta}$ measurement obtained from the LRGs and the ideal measurement. In this case, noise substantially degrades even the single-tracer version of the measurement. Splitting the sample into high and low bias parts (we assume $b = 1.5$ and $b = 2.3$) results in a completely negligible improvement, and adding the LRGs on top of a perfect unbiased tracer does not improve the results much (beyond the unbiased tracer results). Figure 9 also shows the absolute results for $P_{\theta\theta}$, β , and α . While the $P_{\theta\theta}$ and β figures are largely provided as a reference for how well a single-tracer can do on these quantities, the lower right panel of Fig. 9 shows that the α measurement for the sample split in half could be an interesting exercise. The bias ratio can be measured to about 2% at $k \simeq 0.05 h \text{ Mpc}^{-1}$, or 1% at $k \simeq 0.1 h \text{ Mpc}^{-1}$. This should be precise enough to place interesting constraints on the form of non-linear bias.

The SDSS main galaxy sample is generally not as good for LSS as the LRGs, because it covers only low redshift and thus much less volume; however, it does have the higher number density that we look for to make the multi-tracer method powerful. [24] provide a realistic split into blue and red samples with bias ratio 0.7, each with $\bar{n} \simeq 0.0044 (h^{-1} \text{ Mpc})^{-3}$ at $z < 0.1$ (center of volume $z \simeq 0.08$). We take $b = 0.9$ and $b = 1.3$. This sample covers only 0.026 cubic Gpc/h. Fig. 10 shows that the multi-tracer approach to measuring $P_{\theta\theta}$ is quite effective at this number density. Unfortunately, the upper right panel of Fig. 10 shows that the absolute measurement still is not very good, requiring one to go to $k_{\max} > 0.1$ just to get a $3 - \sigma$ level of detection, and to $k_{\max} > 0.3$ to measure $P_{\theta\theta}$ to 10% (which is surely not possible at low z because of non-linearity). The situation with β is similar, but it is again interesting to note, in the lower right of Fig. 10, that the bias ratio for the realistic split sample can be measured to a few percent. One should keep in mind however that at high k the tracers are not maximally correlated and this weakens the constraints. Cosmological simulations will be needed to address this in more detail.

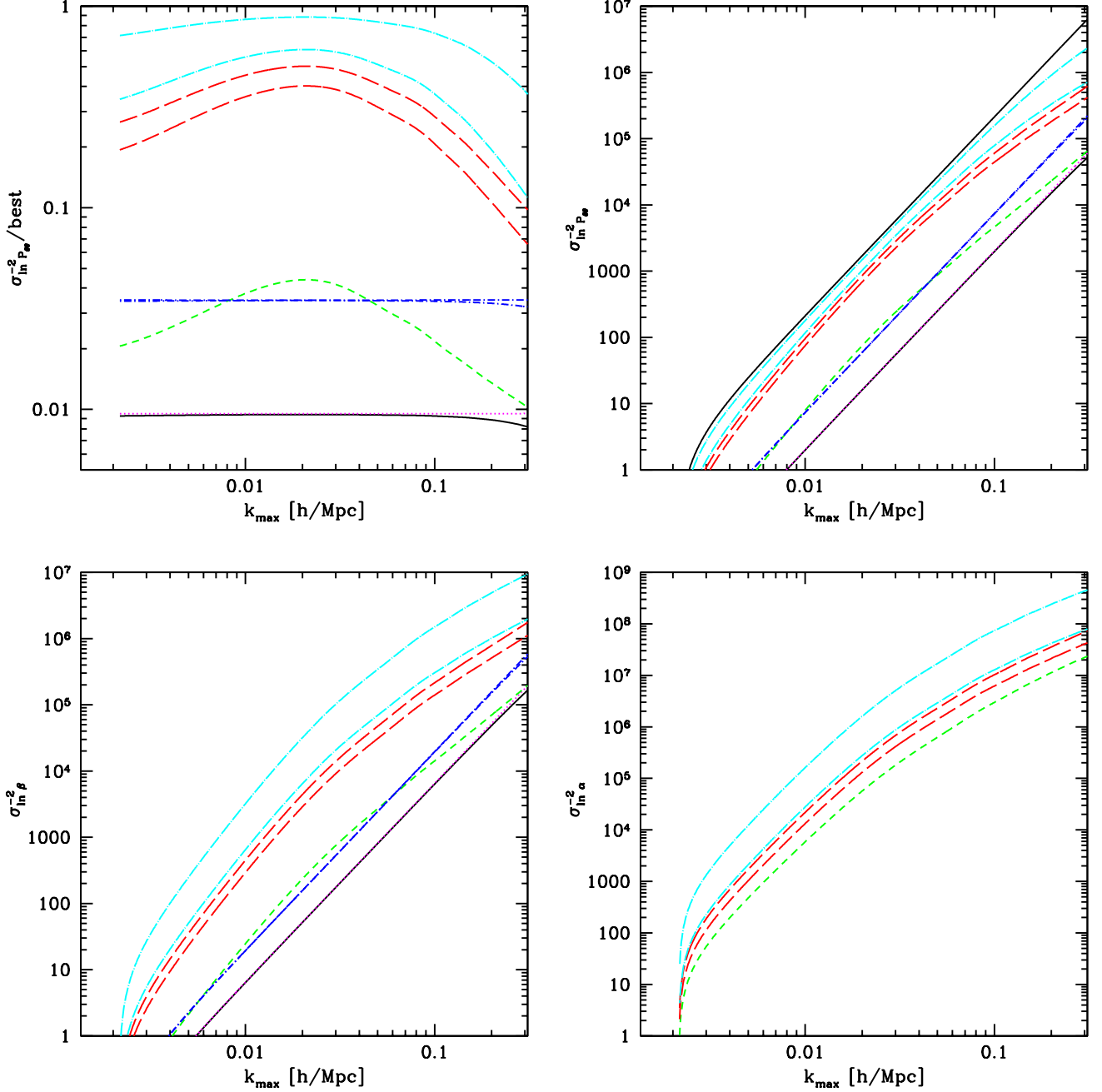


FIG. 7: Upper left panel: Projected error (inverse variance) on the normalization of $P_{\theta\theta} \equiv f^2 P_m$, relative to the error one could achieve by observing velocity divergence directly (or using two perfect tracers with different bias), as a function of k_{\max} , for the SNAP mission-motivated example described in the text. The black (solid) line shows SNAP-like galaxies treated as a single tracer. The magenta (dotted) and blue (dot-short-dashed) lines show single perfectly sampled tracers with $b = 2.3$ and $b = 1$, respectively. Green (short-dashed) shows the SNAP-like galaxies split into two groups with different bias, as described in the text. Red (long-dashed) shows the SNAP-like galaxies plus a perfect unbiased tracer, while cyan (dot-long-dashed) shows a density $\bar{n} = 0.03 (h^{-1} \text{Mpc})^{-3}$ plus an unbiased tracer. Where there are two lines of the same type, the upper one uses a genuinely perfectly sampled tracer, while the lower one shows density $\bar{n} = 0.03 (h^{-1} \text{Mpc})^{-3}$. The other panels are related to the upper left as in Fig. 6.

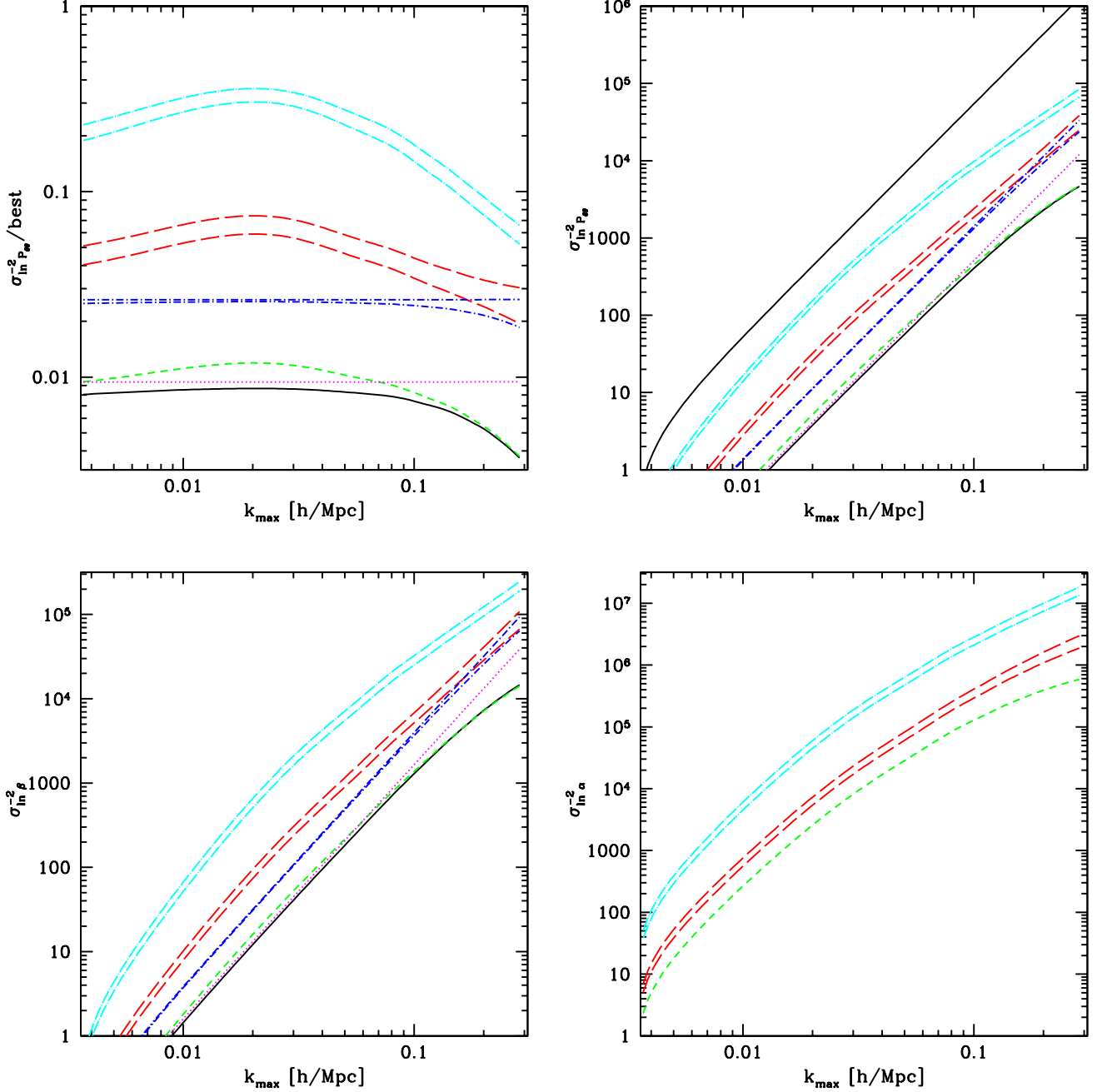


FIG. 8: Upper left panel: Projected error (inverse variance) on the normalization of $P_{\theta\theta} \equiv f^2 P_m$, relative to the error one could achieve by observing velocity divergence directly, or with two perfectly sampled tracers, similar to Fig. 6, except this is for the SDSS-III/BOSS-galaxy-related example described in the text. The black (solid) line shows BOSS galaxies treated as a single tracer. The magenta (dotted) and blue (dot-short-dashed) lines show single perfect tracers with $b = 1.9$ and $b = 1$, respectively. Green (short-dashed) shows the BOSS galaxies split into two groups with different bias, as described in the text. Red (long-dashed) shows the SDSS-III galaxies plus a perfect unbiased tracer, while cyan (dot-long-dashed) shows ten times the BOSS galaxy density plus a perfect unbiased tracer. Where there are two lines of the same type, the upper one uses a genuinely perfectly sampled tracer, while the lower one shows density $\bar{n} = 0.003 (h^{-1} \text{Mpc})^{-3}$ (long-dashed and dot-short-dashed) or $\bar{n} = 0.03 (h^{-1} \text{Mpc})^{-3}$ (dot-long-dashed). The other panels are related to the upper left as in Fig. 6.

C. Beyond redshift-space distortions

So far, primarily for the purpose of transparency of the presentation, the only information we have used from galaxy surveys is the BAO scale and $P_{\theta\theta}(z, k = 0.1 h \text{ Mpc}^{-1})$, as measured from redshift-space distortions, ignoring other effects on the galaxy power spectrum. Generally, however, several other obvious effects should be included: The power spectrum cannot be observed in $h^{-1} \text{ Mpc}$ units, so the conversion to velocity (redshift) coordinates, $\Delta v = H(a) a \Delta x_{\parallel}$, and angular coordinates, $\Delta\theta = D_A(a)^{-1} a \Delta x_{\perp}$, must be accounted for. The uncertainty in the component of these conversions that takes one from angular coordinates to velocity coordinates, $H(a)D_A(a)$, is often called the Alcock-Paczynski effect [17]. In addition to the transformation to observable coordinates, cosmological parameters generally affect the scale dependence of the power spectrum through the transfer function between early-time perturbations from inflation and the linear theory perturbations that we see, e.g., the classic $\Gamma = \Omega_{m,0}h$ scale for the turnover of the power spectrum. In Figure 11 we show the constraining power for the same general 3/4-sky survey up to z_{max} that we have discussed before, except now computing the Fisher matrix using the full parameter dependence of the power spectrum. Note that the BAO measurement is automatically included within this framework, although in a somewhat weaker than usual form because of our relatively conservative k_{max} cut. The extra parameter dependence leads to typically a factor 3-5 larger FoM than one would find using $f^2 P_m$ and BAO constraints alone. There is a new feature at high S/N, however, in that we no longer find any cosmic variance limit on the constraining power! The measurement can be improved arbitrarily much if the S/N can be improved, but to achieve these improvements the number density of tracers must greatly exceed current designs.

In Fig. 11 we also explore the complementarity of weak gravitational lensing measurements, as represented by the DETF Stage IV space (SNAP) or ground (LSST) projections (we use their optimistic versions). We see that these experiments, in combination with Planck (and all Stage II experiments, although these play a minor role), can achieve an FoM improvement of about a factor of 10 over the baseline. Redshift surveys are at best comparable if they are limited to BAO, but they can potentially greatly exceed this if all information at $k_{\text{max}}(z) = 0.1 [D(z)/D(0)]^{-1} h \text{ Mpc}^{-1}$ can be used.

III. NON-GAUSSIANITY

Many of the non-standard models of how the primordial structure was seeded predict non-Gaussianity of local type, $\Phi = \phi + f_{\text{NL}}\phi^2$, where Φ is the gravitational potential in the matter era and ϕ is the corresponding primordial Gaussian case. The effect of this type of initial conditions on the galaxy power spectrum was recently computed by [15] and further investigate by [25, 26, 27, 28]. The effect was used to place observational limits on f_{NL} by [29]. We can easily generalize the [14] multi-tracer error on the non-Gaussianity parameter f_{NL} to the more transparent approach of this paper. In that case, where redshift-space distortions have so far been ignored, the perturbations of galaxy type i can be written

$$\delta_{gi} = (b_i + c_i f_{\text{NL}}) \delta + n_i \quad (16)$$

where c_i is an ideally known coefficient characterizing the galaxy type's response to non-Gaussianity (called $\Delta b(k)$ by [14], with $\Delta b_i(k) = 3(b_i - p_i) \delta_c \Omega_m H_0^2 / c^2 k^2 T(k) D(z)$ from a model for clustering of halos – see [14] for an explanation). The model we will use for perturbations of two types of galaxies is

$$\delta_{g1} = b \left(1 + c_1 \tilde{f}_{\text{NL}} \right) \delta + n_1, \quad (17)$$

where $\tilde{f}_{\text{NL}} = f_{\text{NL}}/b$, and

$$\delta_{g2} = b \left(\alpha + c_2 \tilde{f}_{\text{NL}} \right) \delta + n_2. \quad (18)$$

Note that the quantity we can measure precisely is not really f_{NL} but instead $\tilde{f}_{\text{NL}} = f_{\text{NL}}/b$. If one is trying to calculate the detection limit, as in [14], then the error on b is irrelevant, but for actual constraints on its value once it is detected the degeneracy between b and f_{NL} becomes relevant. Like [14], we start by assuming that α is measured precisely from relatively small scales where the non-Gaussian effect is small, and c_i are known, so we only have two free parameters, $P \equiv 2 b^2 \langle \delta^2 \rangle$, and \tilde{f}_{NL} . The Fisher matrix for a single mode can be inverted to give the error on \tilde{f}_{NL} , in the low noise, small \tilde{f}_{NL} limit:

$$\sigma_{\tilde{f}_{\text{NL}}}^2 = \frac{X_{11} - 2X_{12} + X_{22}}{(c_1 - \alpha^{-1}c_2)^2}, \quad (19)$$

where, again, $X_{ij} = N_{ij}/b_i b_j P_m$. This result is the same as in [14], once we account for differences in definitions.

Estimates of the improvement factor for specific surveys in [14] are somewhat optimistic, because the improvement factor was evaluated using the signal-to-noise ratio at $k = 0.01 h \text{ Mpc}^{-1}$, near the peak of the power spectrum. This will give the correct improvement factor for a measurement using modes on that scale, but, as shown by [25], it is larger scale modes, where the signal-to-noise ratio for fixed noise will be lower, that will give the most interesting constraints on f_{NL} . It is also not obvious when the assumption that P and α are perfectly measured using higher k data is safe. It seems useful to recalculate the constraints in the slightly more general approach we used for redshift-space distortions, i.e., including α as a free parameter and integrating over k up to some k_{max} . The results are shown in Figs 12 and 13. Fig. 12 shows the same SDSS-III scenarios discussed for constraints on β . For the single galaxy type case, we expect an error $b \sigma_{\tilde{f}_{\text{NL}}} \sim 21$, as long as we can use modes up to $k_{\text{max}} \sim 0.05 h \text{ Mpc}^{-1}$. Note that the need to marginalize over the amplitude leads to a $\sim 33\%$ expansion in the errors. The improvement when the sample is split into high and low bias parts is modest, with $b \sigma_{\tilde{f}_{\text{NL}}} \sim 17$. This is consistent with the finding of [14]. Adding a perfect unbiased tracer helps substantially more, allowing a measurement to $b \sigma_{\tilde{f}_{\text{NL}}} \sim 7.3$, again consistent with the improvement factor of [14]. The marginalization over nuisance parameters has led to a $\sim 45\%$ increase in the error.

Fig 13 shows the f_{NL} constraints for the EUCLID-like scenario, as discussed for β . With only a single tracer, we expect an error $b \sigma_{\tilde{f}_{\text{NL}}} \sim 2.0$, as long as we can use modes up to $k_{\text{max}} \sim 0.05 h \text{ Mpc}^{-1}$. A simple split of the sample could improve this significantly, to 1.4 (note that [14] assumed a factor of two higher galaxy density for his high redshift example, corresponding to the original SPACE plan, and so found a somewhat larger enhancement factor). The enhancement when a perfect unbiased tracer is added is dramatic, $b \sigma_{\tilde{f}_{\text{NL}}} \sim 0.54$. In order to produce a solid detection for $f_{\text{NL}} < 1$, we would need either a higher number density, e.g., like the SNAP sample we discussed above (except over a larger volume), or we would need to go to higher redshift where there is more volume, as discussed by [14, 25, 26].

IV. DISCUSSION AND CONCLUSIONS

Galaxy redshift surveys allow one to measure the 3-dimensional distribution of galaxies, which contains an enormous amount of information compared to the 2-dimensional surveys such as cosmic microwave background anisotropies or weak lensing. Their main limitation is that we cannot directly determine the bias b which relates galaxies to the dark matter. In this paper we propose a new method to measure the redshift space distortion parameter $\beta = f/b$, where b is the tracer bias, $f = d \ln D / d \ln a$, D is the growth factor and a the expansion factor. The method is based on angular dependence (with respect to the line of sight) of relative clustering amplitude of two tracers with different bias. In such a ratio the dependence on the mode amplitude vanishes and the method circumvents the usual cosmic variance limit caused by random nature of the modes. This allows one to determine the relative bias to an accuracy that is only limited by the number density of tracers. In principle this allows one to determine the velocity divergence power spectrum $P_{\theta\theta}$ as precisely as one would by directly measuring the velocity divergence itself. This, in turn, would allow for a high precision determination of growth of structure as a function of redshift, as encoded in fD . A high density redshift survey of galaxies would allow for a more precise determination of dark energy parameters, as encoded in DETF Figure of Merit, than any other currently proposed Stage IV experiment.

To achieve these gains one needs low noise, which in turn requires high density of galaxies for both samples. Roughly, the method requires $\bar{n} P_g \gg 1$, where \bar{n} is the number density and $P_g(k)$ is the galaxy power spectrum amplitude. However, most of the existing and planned BAO redshift surveys strive for $\bar{n} P_g \sim 1$, since one does not gain much in the galaxy power spectrum error once the field is significantly oversampled (i.e. $\bar{n} P_g \gg 1$). Most redshift surveys only try to measure the shape of the power spectrum (in search of baryonic acoustic oscillations and other features) and not its amplitude. As long as survey speed is limited by the rate of observing individual objects (e.g., doubling the number density means halving the volume), the correct strategy will probably be to observe the full sky at the usual optimal BAO density, and then to go back to observe at higher density if possible.

In addition to very precise measurements of β , this multiple tracer method will allow precise consistency checks of the model. As one example, we can measure the bias ratio as a function of scale without cosmic variance and therefore study the onset of nonlinear bias. As another example, we can test the redshift space distortion model by fitting for a parameter β' of the distortion model $(1 + \beta \mu^2 + \beta' \mu^4)$, to verify that $\beta' = 0$. This new parameter β' can also be measured to the same in principle bottomless level of precision as β .

In the short term, the technique in this paper will be most useful if methods are found that can achieve high effective number density without sacrificing volume, e.g., 21cm emission mapping [20]. Suppose one had a single perfectly sampled, high resolution field, say, from 21 cm emission mapping [20]. One can always create a second, biased field by some simple non-linear transformation, like squaring the original field, or taking just the high sigma peaks of the field. It may seem impossible that this could gain one any information, and that would be true if one was able to theoretically describe and exploit the field on all scales, including using higher order statistics; however,

when one is otherwise limited to only very large scales this approach can add information, because it makes selective use of small-scale information, exploiting our understanding from renormalization of perturbation theory that local non-linear transformations of the density field can do nothing but change the bias parameters on large scales [19, 25]. Another way to see that this can work is simply to note that the two types of galaxy fields we have been discussing are simply two different non-linear transformations by nature of the same underlying density field, i.e., there is no reason we cannot do the same thing artificially. One would need to keep in mind in this approach that the transformation is applied to the redshift-space field, unlike standard bias which is a transformation of the real-space field. For the f_{NL} application this is unlikely to be a fatal problem, but it may be for the redshift-space distortion measurement discussed in this paper.

Our results suggest that there is much more to be gained by oversampling the density field and that one can determine the growth of structure as a function of redshift to a higher accuracy than previously believed. It is thus worth revisiting the planning of redshift surveys in light of these results. There is every reason to believe that these measurements can be made very robustly. We have boiled the constraint from a galaxy survey at a single redshift down to one number, but we will still have the full scale and angular dependence of the power spectrum, along with higher order statistics, to help us verify that there is nothing about the modeling that we do not understand. In addition, a realistic assessment would also need to address the issue of stochasticity between the tracers with numerical simulations, which would determine the value of k_{max} beyond which the two tracers are not strongly correlated anymore. Preliminary results suggest this is around $k_{\text{max}} \sim 0.1 h \text{ Mpc}^{-1}$ [30], but a more detailed analysis of multi-tracer method with simulations is needed, similar to the recent analysis of single tracer method [13]. We leave this subject to a future work.

Another promising direction is to combine our no cosmic variance measurement of $\beta = f/b$ with an analogous measurement of bias b using a comparison of weak lensing and galaxy clustering [31], to derive $f(z)$ alone without any cosmic variance limitation. We leave these subjects to a future work.

We thank Ue-Li Pen, Nikhil Padmanabhan and Martin White for helpful discussions. U.S. is supported by the Packard Foundation, DOE and Swiss National Foundation under contract 200021-116696/1.

-
- [1] A. Albrecht, G. Bernstein, R. Cahn, W. L. Freedman, J. Hewitt, W. Hu, J. Huth, M. Kamionkowski, E. W. Kolb, L. Knox, et al., ArXiv Astrophysics e-prints (2006), astro-ph/0609591.
 - [2] H. Hoekstra, L. van Waerbeke, M. D. Gladders, Y. Mellier, and H. K. C. Yee, *Astrophys. J.* **577**, 604 (2002).
 - [3] E. S. Sheldon, D. E. Johnston, J. A. Frieman, R. Scranton, T. A. McKay, A. J. Connolly, T. Budavári, I. Zehavi, N. A. Bahcall, J. Brinkmann, et al., *AJ* **127**, 2544 (2004).
 - [4] U. Seljak, A. Makarov, R. Mandelbaum, C. M. Hirata, N. Padmanabhan, P. McDonald, M. R. Blanton, M. Tegmark, N. A. Bahcall, and J. Brinkmann, *Phys. Rev. D* **71**, 043511 (2005).
 - [5] L. Verde, A. F. Heavens, W. J. Percival, S. Matarrese, C. M. Baugh, J. Bland-Hawthorn, T. Bridges, R. Cannon, S. Cole, M. Colless, et al., *MNRAS* **335**, 432 (2002).
 - [6] E. Hawkins, S. Maddox, S. Cole, O. Lahav, D. S. Madgwick, P. Norberg, J. A. Peacock, I. K. Baldry, C. M. Baugh, J. Bland-Hawthorn, et al., *MNRAS* **346**, 78 (2003), arXiv:astro-ph/0212375.
 - [7] W. J. Percival, D. Burkey, A. Heavens, A. Taylor, S. Cole, J. A. Peacock, C. M. Baugh, J. Bland-Hawthorn, T. Bridges, R. Cannon, et al., *MNRAS* **353**, 1201 (2004), arXiv:astro-ph/0406513.
 - [8] M. Tegmark, D. J. Eisenstein, M. A. Strauss, D. H. Weinberg, M. R. Blanton, J. A. Frieman, M. Fukugita, J. E. Gunn, A. J. S. Hamilton, G. R. Knapp, et al., *Phys. Rev. D* **74**, 123507 (2006), arXiv:astro-ph/0608632.
 - [9] L. Guzzo, M. Pierleoni, B. Meneux, E. Branchini, O. Le Fèvre, C. Marinoni, B. Garilli, J. Blaizot, G. De Lucia, A. Pollo, et al., *Nature (London)* **451**, 541 (2008), arXiv:0802.1944.
 - [10] J. Yoo, J. L. Tinker, D. H. Weinberg, Z. Zheng, N. Katz, and R. Davé, *Astrophys. J.* **652**, 26 (2006), arXiv:astro-ph/0511580.
 - [11] E. Sefusatti, M. Crocce, S. Pueblas, and R. Scoccimarro, *Phys. Rev. D* **74**, 023522 (2006), astro-ph/0604505.
 - [12] Y.-S. Song and W. J. Percival, ArXiv e-prints **807** (2008), 0807.0810.
 - [13] W. J. Percival and M. White, ArXiv e-prints **808** (2008), 0808.0003.
 - [14] U. Seljak, ArXiv e-prints **807** (2008), 0807.1770.
 - [15] N. Dalal, O. Doré, D. Huterer, and A. Shirokov, *Phys. Rev. D* **77**, 123514 (2008), 0710.4560.
 - [16] A. Slosar, ArXiv e-prints (2008), 0808.0044.
 - [17] C. Alcock and B. Paczynski, *Nature (London)* **281**, 358 (1979).
 - [18] N. Kaiser, *MNRAS* **227**, 1 (1987).
 - [19] P. McDonald, *Phys. Rev. D* **74**, 103512 (2006).
 - [20] T.-C. Chang, U.-L. Pen, J. B. Peterson, and P. McDonald, *Physical Review Letters* **100**, 091303 (2008), arXiv:0709.3672.
 - [21] M. Crocce and R. Scoccimarro, *Phys. Rev. D* **73**, 063520 (2006).
 - [22] H.-J. Seo and D. J. Eisenstein, *Astrophys. J.* **665**, 14 (2007), arXiv:astro-ph/0701079.

- [23] A. Cimatti, M. Robberto, C. Baugh, S. V. W. Beckwith, R. Content, E. Daddi, G. De Lucia, B. Garilli, L. Guzzo, G. Kauffmann, et al., *Experimental Astronomy* pp. 12–+ (2008), arXiv:0804.4433.
- [24] M. E. C. Swanson, M. Tegmark, M. Blanton, and I. Zehavi, *MNRAS* **385**, 1635 (2008), arXiv:astro-ph/0702584.
- [25] P. McDonald, ArXiv e-prints, 0806.1061 (2008).
- [26] N. Afshordi and A. J. Tolley, ArXiv e-prints, 0806.1046 (2008).
- [27] S. Matarrese and L. Verde, *ApJ* **677**, L77 (2008), arXiv:0801.4826.
- [28] C. Carbone, L. Verde, and S. Matarrese, *ApJ* **684**, L1 (2008), 0806.1950.
- [29] A. Slosar, C. Hirata, U. Seljak, S. Ho, and N. Padmanabhan, *Journal of Cosmology and Astro-Particle Physics* **8**, 31 (2008), 0805.3580.
- [30] U. Seljak and M. S. Warren, *MNRAS* **355**, 129 (2004), arXiv:astro-ph/0403698.
- [31] U.-L. Pen, *MNRAS* **350**, 1445 (2004), arXiv:astro-ph/0402008.
- [32] www.sdss3.org

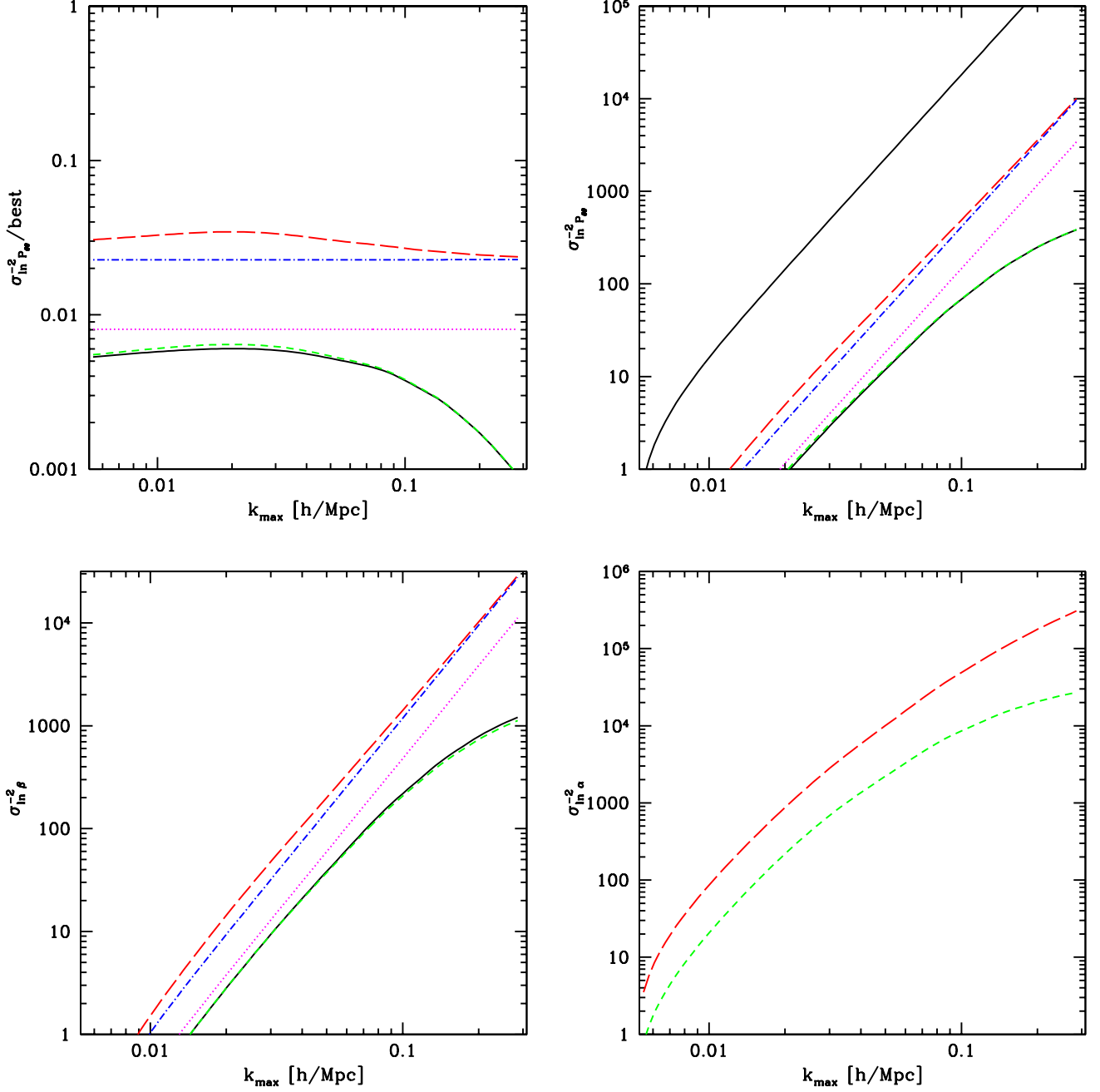


FIG. 9: Upper left panel: Projected error (inverse variance) on the normalization of $P_{\theta\theta} \equiv f^2 P_m$, relative to the error one could achieve by observing velocity divergence directly, or with two perfectly sampled tracers, similar to Fig. 6, except this is for the current SDSS LRGs. The black (solid) line shows LRGs as a single tracer. The magenta (dotted) and blue (dot-short-dashed) lines show single perfect tracers with $b = 1.9$ and $b = 1$, respectively. Green (short-dashed) shows the LRGs galaxies split into two groups with different bias, as described in the text. Red (long-dashed) shows the LRGs plus a perfect unbiased tracer. The other panels are related to the upper left as in Fig. 6.

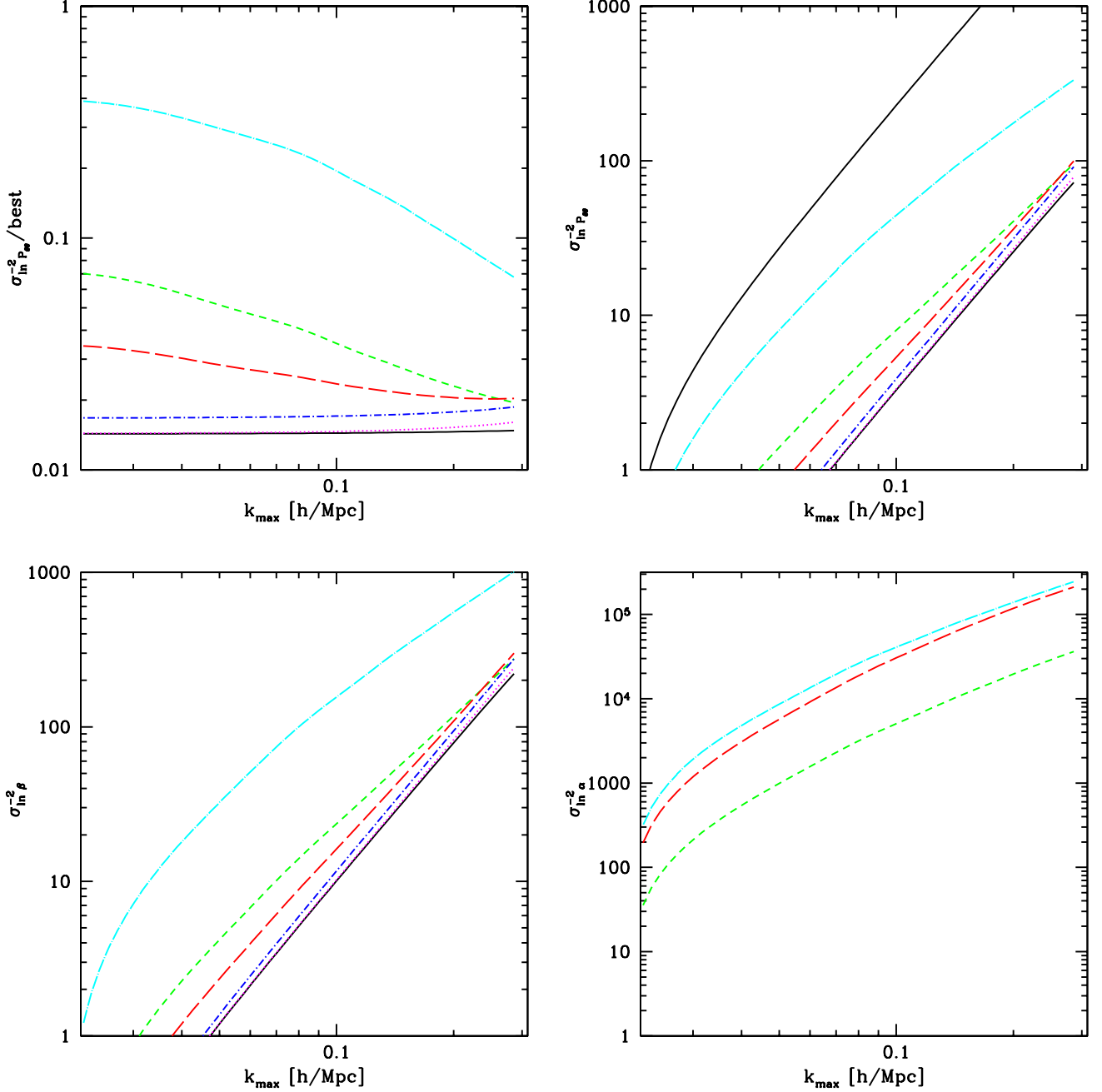


FIG. 10: Upper left panel: Projected error (inverse variance) on the normalization of $P_{\theta\theta} \equiv f^2 P_m$, relative to the error one could achieve by observing velocity divergence directly, or with two perfectly sampled tracers, similar to Fig. 6, except this is for the current SDSS main galaxies. The black (solid) line shows SDSS galaxies as a single tracer. The magenta (dotted) and blue (dot-short-dashed) lines show single perfect tracers with $b = 1.1$ and $b = 1$, respectively. Green (short-dashed) shows the main galaxies split into two groups with bias $b = 1.3$ and $b = 0.9$, both with $\bar{n} = 0.0044 (h^{-1} \text{Mpc})^{-3}$, as described in the text. Red (long-dashed) shows the main galaxies plus a perfect unbiased tracer. Cyan (dot-long-dashed) shows two tracers with $b = 1.3$ and $b = 0.9$, both with $\bar{n} = 0.044 (h^{-1} \text{Mpc})^{-3}$. The other panels are related to the upper left as in Fig. 6.

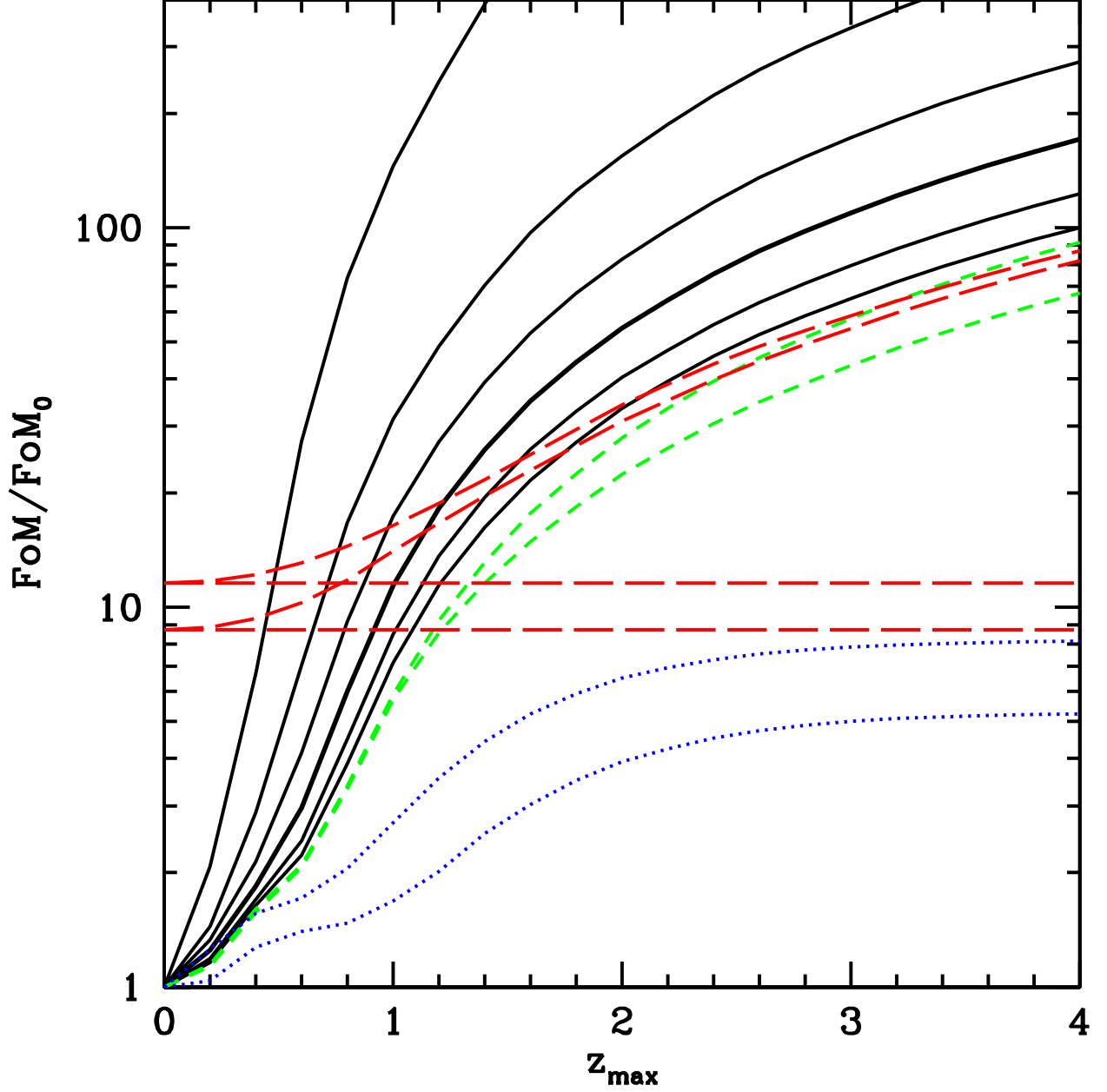


FIG. 11: Improvement in DETF FoM when all of the information in the redshift-space power spectrum is used rather than just BAO and $f^2 P_m$ constraints, for $k_{\text{max}}(z) = 0.1 [D(z)/D(0)]^{-1} h \text{Mpc}^{-1}$ (relative to Planck+Stage II, and for 30000 sq. deg., as usual). Green (dashed) lines show single $S/N=1$ (at $k = 0.4 h \text{Mpc}^{-1}$) tracers with $b = 1$ (upper) and $b = 2$ (lower). The black curves show both types of galaxy together, each with (bottom to top) $S/N=1, 3, 10, 30, 100, 1000$ (the constraining power increases without bound as the S/N improves). Blue (dotted) shows BAO alone, with the lower curve using the above k_{max} and the upper curve using smaller scales as described in [22] (the rest of the curves effectively use the weaker version). The red (long-dashed) curves include weak lensing constraints, with the lower two (horizontal) lines including no redshift survey (lowest is approximately as SNAP weak lensing, 2nd lowest is LSST weak lensing), while the upper two include the $b = 2$ -only (weakest) redshift survey.

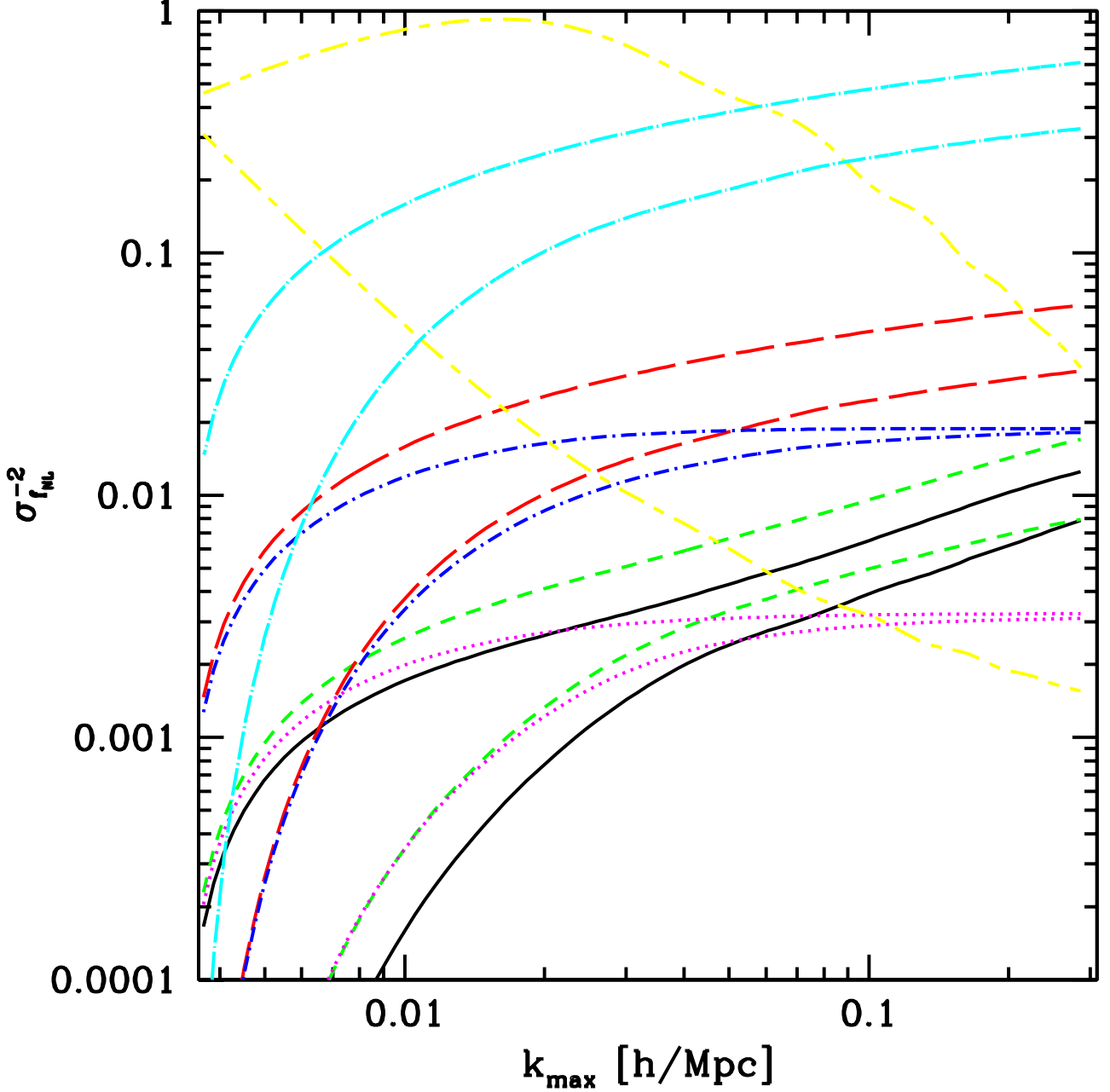


FIG. 12: Projected f_{NL} errors (inverse variance) as a function of k_{max} , for the SDSS-III/BOSS galaxy example described in the text. Strictly speaking, this is not $\sigma_{f_{\text{NL}}}$ but instead $b \sigma_{\tilde{f}_{\text{NL}}}$, where $\tilde{f}_{\text{NL}} = b^{-1} f_{\text{NL}}$, but the distinction is irrelevant for a rough detection limit. In each case, the lower curve of a type is marginalized over P and α , while the upper curve is not. Black (solid) assumes BOSS alone, treated as a single tracer. Green (short-dashed) curves show the case when the BOSS galaxies are split into high and low bias subsamples, as described in the text, while magenta (dotted) curves are the same except the transfer function is ignored when computing the non-Gaussian effect, restricting it to large scales. Red (long-dashed) show an infinite S/N, unbiased, tracer added to BOSS, while blue (dot-short-dashed) show the same with no transfer function effect in the calculation of the non-Gaussian signal. Cyan (dot-long-dashed) shows a perfect unbiased tracer added to a tracer with $b = 1.9$ and ten times the BOSS number density. The yellow (short-dash-long-dash) curves do not show errors on f_{NL} , the upper curve shows $(P/2N)/10$, where P is the power spectrum and N is the noise for the full set of BOSS galaxies, and the lower curve $f_{\text{NL}} c(k)/b$ where $c(k)$ is our best guess at the BOSS galaxies' response to non-Gaussianity, b is their bias, and $f_{\text{NL}} = 30$.

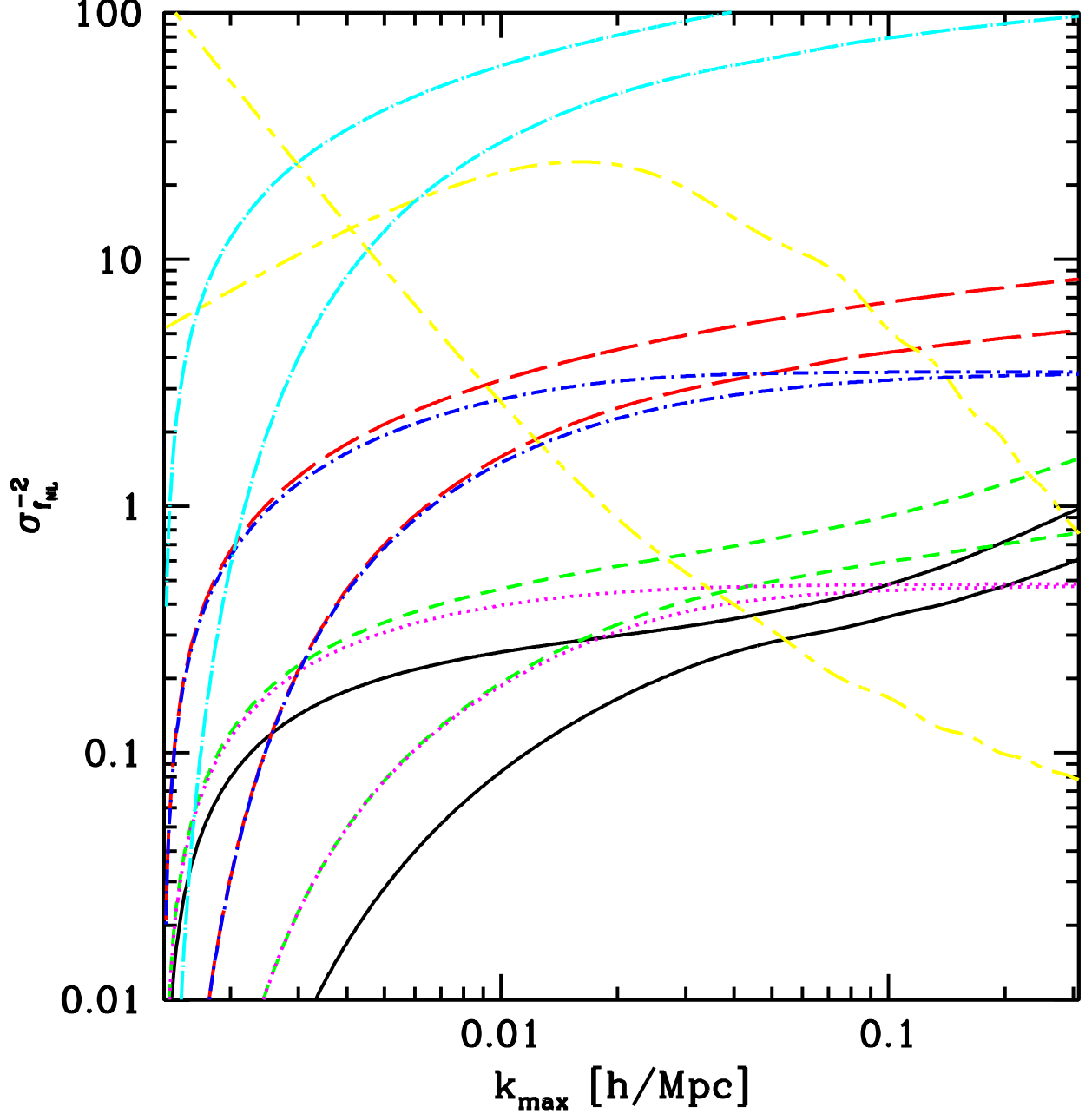


FIG. 13: Projected f_{NL} errors (inverse variance) as a function of k_{max} , similar to Fig. 12, for the EUCLID-like scenario. In each case, the lower curve of a type is marginalized over P and α , while the upper curve is not. Black (solid) assumes EUCLID alone, treated as a single tracer. Green (short-dashed) curves show the case when the EUCLID galaxies are split into high and low bias subsamples, as described in the text, while magenta (dotted) curves are the same except the transfer function is ignored when computing the non-Gaussian effect, restricting it to large scales. Red (long-dashed) show an infinite S/N, unbiased, tracer added to EUCLID, while blue (dot-short-dashed) show the same with no transfer function effect in the calculation of the non-Gaussian signal. Cyan (dot-long-dashed) shows a perfect unbiased tracer added to a tracer with $b = 2$ and ten times the EUCLID number density. The yellow (short-dash-long-dash) curves do not show errors on f_{NL} , the upper curve shows $(P/2N)$, where P is the power spectrum and N is the noise for the full set of EUCLID galaxies, and the lower curve $1000f_{\text{NL}}c(k)/b$ where $c(k)$ is our best guess at the EUCLID galaxies' response to non-Gaussianity, b is their bias, and $f_{\text{NL}} = 1$.